ON DISCRIMINATION BETWEEN CARBONATE AND SILICATE INPUTS TO HIMALAYAN RIVERS

MIKE J. BICKLE*,†, ED TIPPER*,**, ALBERT GALY*,§, HAZEL CHAPMAN*, and NIGEL HARRIS***

ABSTRACT. We review new and published analyses of river waters, bedloads and their constituent minerals from the Dhauli Ganga and Alaknanda, headwaters of the Ganges in Garhwal, and the Marsyandi in Nepal and their tributaries. These data are used to discriminate between the inputs of major cations and Sr from silicate and carbonate sources. Methods of estimating the proportion of the carbonate and silicate inputs to river waters using mixing arrays in Sr-Ca-Mg-Na-K-^{87}Sr/^{86}Sr space are shown to suffer from systematic correlations between the magnitude of the precipitation of secondary calcite and the fraction of the silicate component. This results in factor-of-two overestimates of the fractions of silicate-derived Ca, Mg and Sr. To correct for this the magnitude of secondary calcite precipitated and relative fractions of silicate and carbonate-derived cations are instead calculated by modeling the displacement of water compositions from the compositions of the carbonate and silicate components of the bedload in subsets of Sr-Ca-Mg-Na-K-^{87}Sr/^{86}Sr space. The compositions of the carbonate and silicate end-members in the bedload are determined by sequential leaching. The results of this modeling are compared with modeling of the modal mineral inputs to waters where mineral compositions are derived from electron-microprobe analyses of the minerals in the bedload. In the upper Marsyandi catchment, which drains low-grade Tethyan Sedimentary Series formations, a set of mainstem samples collected over a two-year period define tight correlations in Sr-Ca-Mg-Na-K-^{87}Sr/^{86}Sr space. Modeling of the magnitude of secondary carbonate precipitation and fractions of silicate-derived Ca, Mg and Sr in Sr-Ca-Mg-^{87}Sr/^{86}Sr space gives self-consistent results that are compatible with both the calculations of mineral modes and published Mg-isotopic compositions, if the ratio of chlorite to biotite weathering is high or if there is another silicate source of Mg. These calculations imply that between 12 and 31 percent of the Sr and 44 and 72 percent of the Mg is derived from silicate minerals where the range reflects the seasonal change in the ratio of silicate-derived to carbonate-derived cations. Modeling in Sr-Ca-Na and/or K space is inconsistent with the Sr-isotopic and Mg-isotopic constraints and we conclude that in this catchment dissolution of Na and K are incongruent relative to Sr-Ca-Mg. Potassium is preferentially retained in micas whereas the controls on Na are unclear. Modeling of the catchments underlain by High Himalayan Crystalline and Lesser Himalayan Series in Garhwal is complicated by the presence of dolomite as well as calcite in the carbonate and the results imply that dolomite dissolves faster in the acetic acid leaches than in nature. Up to 60 percent of the Sr in the catchment on High Himalayan Crystalline Series and 20 to 30 percent of Sr in the catchments on Lesser Himalayan Series are estimated to be derived from silicates. However it should be noted that the element budgets are not all self-consistent and the use of bedrock-element ratios to model the sources of chemical inputs to river waters remains subject to uncertainties.

Key words: chemical weathering, silicate weathering, river chemistry, Himalayas, Sr-isotopes

* Department of Earth Sciences, University of Cambridge, Downing Street, Cambridge CB2 3EQ, United Kingdom
** Department of Earth Sciences, University of St Andrews, St Andrews, KY16 9AL, Scotland
*** Department of Environment, Earth and Ecosystems, Open University, Milton Keynes MK7 6AA, United Kingdom.
§ Present address: CRPG - CNRS - Université de Lorraine, BP20, 54501 Vandœuvre-lès-Nancy, Cedex, France
† Corresponding author: mb72@esc.cam.ac.uk

The controls on global climate on geological time scales are imperfectly understood. This is well illustrated by controversies over the causes of Cenozoic cooling which has culminated in the current glacial cycles. The cooling from about 50 Ma (Zachos and others, 2001) is coincident with the India-Asia continental collision and subsequent exhumation of the Himalayas and Tibet. This has focussed attention on the possible links between exhumation, erosion, changes in silicate chemical weatherability of the crust, and climate (Chamberlin, 1899; Raymo and others, 1988; Caldeira and others, 1993; Bickle, 1996). Further, the marked rise in oceanic $^{87}Sr/^{86}Sr$ ratios from 40 Ma has also been linked to increased exhumation and chemical weathering of the high $^{87}Sr/^{86}Sr$ ratio rocks in the Himalayas (Edmond, 1992; Richter and others, 1992). However the extent to which this rise relates to weathering of carbonate rocks with elevated $^{87}Sr/^{86}Sr$ ratios or to increased fluxes from weathering of silicate rocks is disputed (for example Edmond, 1992; Palmer and Edmond, 1992; Krishnaswami and others, 1992; Krishnaswami and Singh, 1998; Singh and others, 1998; Galy and others, 1999; Bickle and others, 2003, 2005). Increased chemical weathering of carbonates has no long-term impact on changes in atmospheric CO_2 and climate. A sustained increase in the silicate chemical weathering flux would imply a corresponding increase in the solid-earth CO_2 degassing flux or the atmosphere would become depleted in CO_2 on time scales greater than a few hundred thousand years.

The problem of partitioning the Sr fluxes from the Himalayas between silicate and carbonate sources is exacerbated because the $^{87}Sr/^{86}Sr$ ratios of Himalayan carbonate minerals have been elevated by exchange with silicate minerals during metamorphism precluding simple use of $^{87}Sr/^{86}Sr$ ratios to distinguish the inputs (Palmer and Edmond, 1992; Galy and others, 1999; Bickle and others, 2001; Oliver and others, 2003). This reflects the more general problem in determining atmospheric CO_2-drawdown from the silicate chemical weathering fluxes carried by rivers, that of distinguishing the Ca, Mg and Sr fluxes derived from silicate minerals from the large fluxes of these elements derived from carbonate minerals.

A wide number of approaches have been used to discriminate the fractions of cations derived from silicate and carbonate sources in rivers. These include estimates of the areas and relative weathering rates of silicate and carbonate rocks (for example Berner and others, 1983), estimates calculated by modal decomposition assigning water chemistry to source mineral compositions (for example Garrels and Mckenzie, 1967), estimates based on average element ratios, either of carbonate and silicate rocks or inferred from the water chemistries, (for example by Harris and others, 1998; Krishnaswami and others, 1999; Galy and France-Lanord, 1999; Gaillardet and others, 1999), methods based on the chemical arrays defined by sets of river water samples (for example Singh and others, 1998; Bickle and others, 2005) and methods based on Sr- or Ca-isotope ratios (for example Bickle, 1994; Davenport and others, 2014). As discussed below, all of these methods have shortcomings.

In this paper we use chemical analyses of river waters together with analyses of carbonate leaches and silicate residues from the bedload, and analyses of minerals in the bed load to model the relative dissolved fractions of Sr, Mg and Ca derived from carbonate and silicate minerals. The acid leaches are presumed to reflect the source carbonate rock compositions and the silicate residues from leaching the source silicate rock compositions. The modeling is carried out both by mass balance in subsets of Sr-Ca-Mg-Na-K-$^{87}Sr/^{86}Sr$ composition space and by mineral-mode mass-balance calculations in Si-Al-Ca-Mg-Na-K composition space. This is a much wider range of composition space than previously modeled (for example Singh and others, 1998; Bickle and others, 2005) and allows exploration of the internal consistency of the calculations. We study catchments in all three main litho-tectonic units in the Himalayas, the Tethyan

Sedimentary Series (TSS), the High Himalayan Crystalline Series (HHCS) and the Lesser Himalayan Series (LHS).

The results confirm that: 1) The Himalayan river waters comprise a mixture of at least two sources with differing weathering characteristics (Tipper and others, 2006a, 2006b), 2) up to 80 percent of Ca is precipitated as secondary calcite in the high, cold Tibetan catchments, 3) Ca loss to secondary calcite is proportionally higher during the dry season correlating with the fraction of cations derived from silicate minerals, 4) tributary compositional arrays are rotated by mixing of components which have undergone systematic differences in precipitation of secondary calcite and 5) comparison of dissolved fluxes of silicate-derived Sr-Ca-Mg-Na-K-^{87}Sr/^{86}Sr with their silicate sources indicates that the silicate-derived components dissolve incongruently. The best estimates of the proportion of Sr derived from silicate minerals are ~8, ~23 and ~21 percent in the Alaknanda, Marsyandi and Nar Tethyan Sedimentary Series catchments, about 60 percent in a High Himalayan Crystalline Series catchment and 20 to 30 percent in Lesser Himalayan Series catchments.

STUDY AREAS AND SAMPLING

The samples considered in this study comprise mainstem river waters, tributary waters, bed and suspended loads and bed rock samples collected in the headwaters of the Ganges in the Garhwal Himalaya and in the upper reaches of the Marsyandi north of the Annapurna Range in Nepal (figs. 1 and 2). The catchment in the upper reaches of the Marsyandi in Nepal (fig. 2) was included in the study because there is restricted access to the areas of Tethyan Sedimentary Series in the Garhwal Himalaya.

Sampling in Garhwal was carried out in 1996, 1997, 1998, 2003 and 2004. In Nepal sampling took place during the pre- and late monsoon seasons in 2002. In addition, the mainstem Marsyandi and the Nar rivers were sampled at approximately two-weekly intervals between April 2002 and August 2003 just above their confluence at Koto just downstream of Chame (Tipper, ms, 2006; Wolff-Boenisch and others, 2009). The 1996 to 2003 Garhwal water samples were presented and discussed by Bickle and others, (2001, 2003, 2005) and the Marsyandi water samples by Bickle and others (2005) and Tipper and others, (2006a, 2006b, 2008). New analyses of bedloads, including the results of sequential leaching to determine the composition of the carbonate and silicate components, and electron microprobe analyses of detrital minerals are also presented here.

The headwaters of the Ganges in Garhwal drain the three major lithotectonic units of the Himalayas, the Tethyan Sedimentary Series, the High Himalayan Crystalline Series and the Lesser Himalayas (fig. 1). The Tethyan Sedimentary Series comprise a south-verging thrust complex of mainly low metamorphic grade deformed clastic and carbonate Palaeozoic and Mesozoic rocks and is bounded to the south by the northerly dipping normal fault, the South Tibetan Detachment Zone. This juxtaposes the Tethyan Sedimentary Series against the high metamorphic grade late-Proterozoic para- and ortho-gneisses of the High Himalayan Crystalline Series. The High Himalayan Crystalline Series is in turn thrust south over the lower grade early Proterozoic mainly clastic and carbonate meta-sedimentary rocks of the Lesser Himalayan Series. The geological setting and the substantial previous work on the headwaters of the Ganges is reviewed by Bickle and others (2003). The Himalayan catchments cross an extreme range of climatic and vegetation zones. The Tethyan Sedimentary Series is mainly exposed in the highest areas above 3000 m where there are permanent ice sheets, vegetation is sparse, precipitation limited (<500 mm/yr) and agriculture is very restricted. The High Himalayan Crystalline Series extends from altitudes above 1000 m to nearly 8000 m with very steep slopes. Environments range from pine forests and Alpine meadows to sparsely vegetated rocky and ice covered mountain tops. The Lesser Himalayan Series extends from altitudes of a few hundred
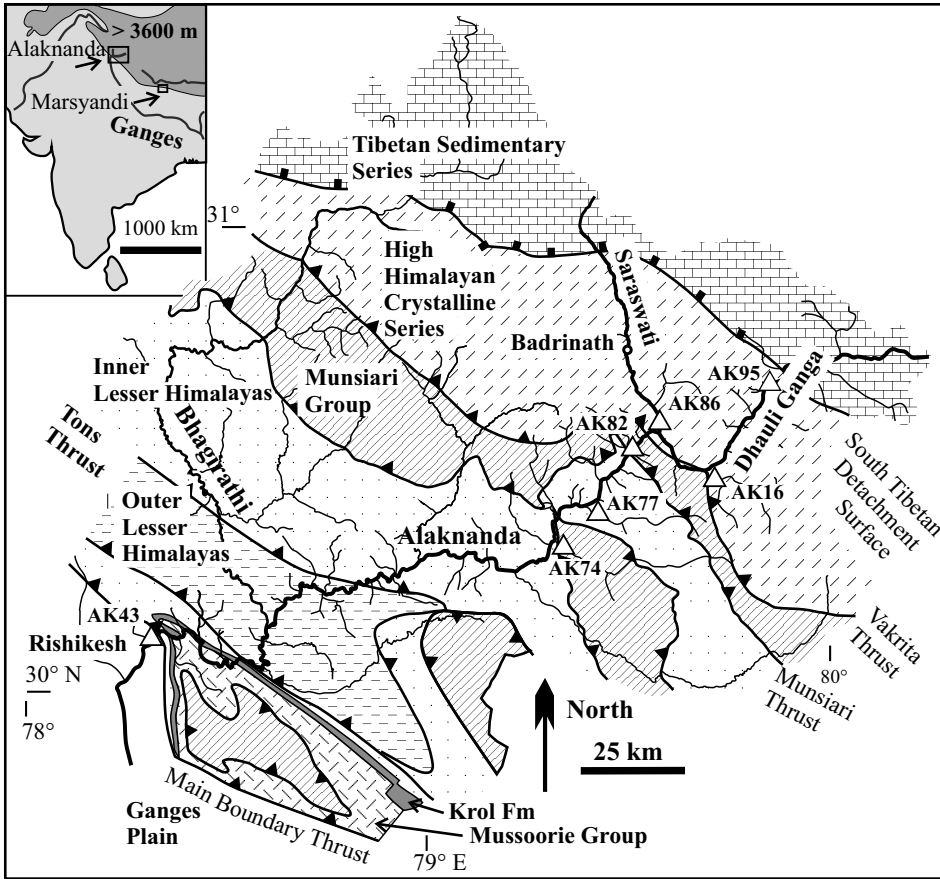
Fig. 1. Geological map of the Alaknanda catchment redrawn after Bickle and others (2005). Location shown on inset along with location of Marsyandi catchment in Nepal (fig. 2). Open triangles show sample sites and sample numbers for river sediment samples subjected to leaching experiments.

meters to ~3700 m; these catchments are often densely forested (oaks, alder, rhododendron), there is significant terracing for agriculture in limited areas, precipitation is high and the climate ranges from sub-tropical at the lowest altitudes to Alpine on the highest peaks. Precipitation is between 1 and 2 m/yr across the High Himalayan Crystalline Series and Lesser Himalayan Series in Garhwal.

The upper reaches of the Marsyandi in Nepal drains mostly Palaeozoic and Mesozoic Tethyan Sedimentary Series lithologies north of the Annapurna Range (fig. 2). The setting is reviewed in more detail by Tipper and others (2006a). The rocks comprise a sequence of limestones and siliclastic units with minor volcanics. Metamorphic grade is generally low except within ~ 3 km of the Southern Tibetan Detachment surface where the grade increases to the biotite zone in pelites with phengite, amphibole and clinopyroxene in calc-silicate rocks. Altitudes in the catchment range from 2500 to 8000 m but are mostly in excess of 4000 m. The cold arid climate is typical of the Tibetan plateau in the rainshadow of the main Himalayan range with monsoonal precipitation less than 0.5 m (Burbank and others, 2003) and minimal vegetation.
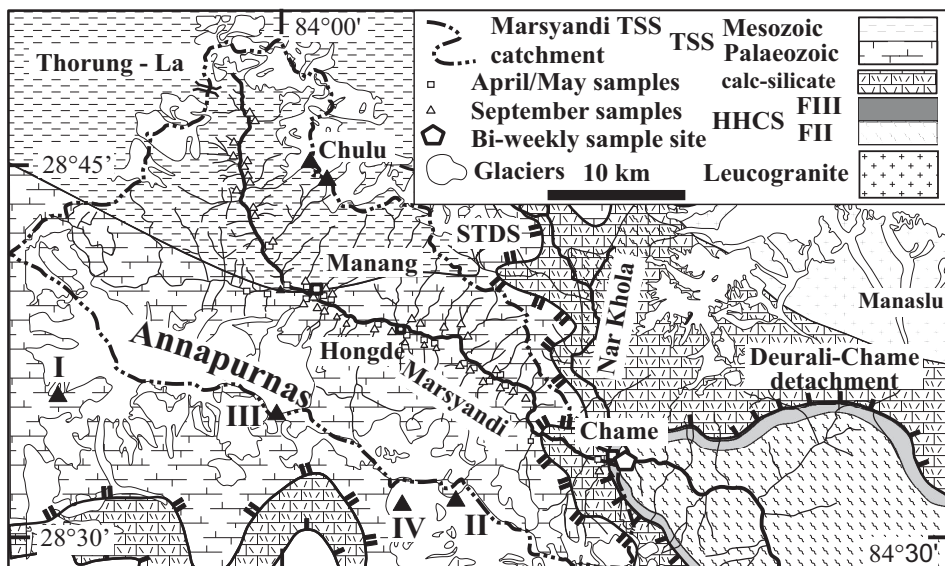
Fig. 2. Geological map of Marsyandi catchment draining the Tethyan Sedimentary Series (TSS) showing site of weekly sampling east of Chame and tributaries sampled. Geology after Colchen and others (1986), as modified by Searle and Godin (2003). Note that the position of the South Tibetan Detachment Zone (STDS) is controversial. The metamorphosed calc-silicate unit between Formation III of the High Himalayan Crystalline Series (HHCS) and Tethyan Sedimentary Series is of uncertain provenance. The Palaeozoic rocks immediately above the South Tibetan Detachment System are metamorphosed to green-schist and lower-amphibolite facies. Location shown on inset on figure 1. **I** to **IV** mark summits of Annapurna.

DATASETS AND ANALYTICAL METHODS

The new analyses of water samples and analytical methods are compiled in supplementary data table S1 (http://earth.geology.yale.edu/~ajs/SupplementaryData/2015/01BickleTables.pdf), analyses and analytical methods of a suite of bed-load samples collected in the headwaters of the Ganges and in the Marsyandi and tributaries above Chame are presented in supplementary data table S2 (http://earth.geology.y-ale.edu/~ajs/SupplementaryData/2015/01BickleTables.pdf) and analyses of leaches and residues from leaching of bedload in supplementary data table S3 (http://earth.geology.yale.edu/~ajs/SupplementaryData/2015/01BickleTables.pdf). Average electron microprobe analyses of detrital minerals are presented in tables 5 and 7 (see below) and table S4 (http://earth.geology.yale.edu/~ajs/SupplementaryData/2015/01BickleTables.pdf) with analytical methods in table S4. The rain and hot-spring corrected water compositions used in the calculations below are listed in table S5 (http://earth.geology.yale.edu/~ajs/SupplementaryData/2015/01BickleTables.pdf).

Bedload samples were taken from exposed bars and comprise sand-sized material. Samples were subjected to sequential leaching in order to recover the cation contents and $^{87}Sr/^{86}Sr$ ratios of the carbonate and silicate fractions (table 1). A variety of published methods were evaluated by leaching mixtures of calcite, dolomite and a silicate sample (KR120: a High Himalayan Crystalline quartzo-feldspathic biotite gneiss with negligible carbonate). None of these methods achieved complete separate leaching of calcite, dolomite and silicate components and the method adopted (table 1) is a compromise between analytical simplicity and effective separation. All the leaching steps were carried out at room temperature with quartz-distilled acids. Cation

Leaching procedures

Stage	Sample	Ultrasonic	Reaction period	Centrifuge		Rinse
Water leach	Add 200 mg fine ground bedload to pre-cleaned centrifuge tube	shake, ultrasonic 10 minutes, shake	2 hours	shake, then 20 minutes in centrifuge	Pipette off water and discard	
Acetic acid leach	Add 5 ml 10% acetic acid to residue from water leach	shake, ultrasonic 10 minutes, shake	> 8 hours (overnight)	shake, then 20 minutes in centrifuge	Pipette off acetic acid into 2 aliquots	Repeat 3 times: add 5 ml water, shake, ultrasonic for 10 minutes, shake, centrifuge for 20 mins, pipette off water and discard.
HCl leach	Add 5 ml 1 molar HCl to residue from acetic acid leach	shake, ultrasonic 10 minutes, shake	> 8 hours (overnight)	shake, then 20 minutes in centrifuge	Pipette off acetic acid into 2 aliquots	Repeat 3 times: add 5 ml water, shake, ultrasonic for 10 minutes, centrifuge for 20 mins, pipette off water and discard.
Residue	Residue from HCl leach heated at 900-950 °C for 8 hours to ignite organics and then taken into solution using HF + HNO_3, HNO_3 and HCl dissolutions in teflon bombs at 180 °C. Aliquots were taken for AES cation and $^{87}Sr/^{86}Sr$ analyses.					

concentrations (Na, K, Ca, Mg, Al, Fe, Mn and Sr) were analyzed on an aliquot of the leaches and residues by ICP-AES with Sr concentrations and $^{87}Sr/^{86}Sr$ ratios measured on a second aliquot spiked with >99 percent pure ^{84}Sr. Comparison of the sum of cation concentrations from leaches and residues with analyses of cation concentrations on the whole bed-load samples by both XRF and ICP-AES confirms the consistency between analytical methods within the ± 5 percent relative analytical errors and that the sum of leaches and residues recovered was 94 ± 6 percent (1σ averaged over all samples and 8 elements) of the whole bedload composition. The calculated $^{87}Sr/^{86}Sr$ ratio of the sum of leaches and residue differed from the whole bed-load $^{87}Sr/^{86}Sr$ ratio by a mean of −0.00026 (1σ ≅ 130). Total procedural Sr blanks were between 200 to 450 pg (the highest blank in the acetic acid stage, the lowest in the HCl stage) and might shift $^{87}Sr/^{86}Sr$ ratios of the lowest Sr concentration HCl leaches by ~0.0001 but are negligible for the other leaching and residue analyses.

The water stage removed cations most probably from mineral surfaces damaged by grinding. Preliminary experiments showed that about 1 percent of the total Sr, but with an $^{87}Sr/^{86}Sr$ ratio intermediate between that of the carbonate and silicate fractions, was removed at this stage. The acetic acid leach removed at least 90 percent of the calcite and at least 50 percent of the dolomite from the synthetic carbonate mixtures. The HCl leach was carried out to remove any residual calcite and much of the residual dolomite. This stage removed between 7 and 25 percent of the Mg (average 18%) and 1 and 3 percent of the total Sr (supplementary data table S3, http://earth.geology.yale.edu/~ajs/SupplementaryData/2015/01BickleTables.pdf). The Sr had an $^{87}Sr/^{86}Sr$ ratio that was elevated compared to mixtures of acetic acid leach and silicate residue suggesting preferential leaching of ^{87}Sr from damaged sites in silicates or from more radiogenic minerals such as micas in addition to any residual carbonate. Na/Ca

and Al/Ca ratios of the HCl leaches imply that the silicate-derived Sr makes a significant contribution to the total Sr in the HCl leach. The small fractions of the Sr, Ca and Mg recovered by the HCl leach suggests that nearly all the calcite and a significant fraction of the dolomite was removed by the acetic leach. HCl leach compositions corrected for silicate inputs by subtracting cations based on the cation/Al ratios of the residue and Al content of the HCl leach (supplementary data table S3) have an average Mg/Ca ratio of 1.4 (range 0.7 to 2.4) suggesting much of the Ca and Mg in the HCl leach is derived from dolomite. Dolomite in Himalayan formations is characteristically low in Sr (<100 ppm) compared with calcite marbles (several hundred ppm) that would reduce the impact of any residual dolomite on the silicate residue composition. The leaching of mixtures of a silicate sample and pure calcite and dolomite mineral fractions suggest that ~1 to 3 percent of the silicate fraction Sr is dissolved in the acetic leach consistent with the Al, Na and K cation concentrations in the acetic acid leaches (table S3). Such levels of cross-contamination will cause a few percent shift in Sr/Ca and Na/Ca ratios. The sensitivity of $^{87}Sr/^{86}Sr$ ratios to cross contamination depends on the relative Sr concentrations of carbonate and silicate and their mass fractions. Thus addition of 1.5 percent Sr from silicate residues to the carbonate fraction makes a negligible difference to the $^{87}Sr/^{86}Sr$ ratio of the acetic acid leach in carbonate-rich samples such as those from the Marsyandi but may shift leaches from the most silicate-rich samples up to ~15 percent towards the $^{87}Sr/^{86}Sr$ ratio of the silicate residue. Conversely retention of 1 percent carbonate Sr in silicate residues would shift measured $^{87}Sr/^{86}Sr$ ratios up to 13 percent towards the carbonate end-member in the most carbonate-rich samples but less than ~1 percent in the silicate-rich bedloads.

Cyclic Inputs

The chemistry of all the water samples used in this paper has been corrected for cyclic inputs by rain and hydrothermal sources based on the conservative behavior of Cl following Bickle and others (2005) (table S5, http://earth.geology.yale.edu/~ajs/SupplementaryData/2015/01BickleTables.pdf). The Cl contents of three June samples from the weekly sampling of the Marsyandi below Chame, for which unacidified samples were not collected, were estimated from a quadratic fit to the Cl/Na ratios of all the Marsyandi time-series samples with Cl analyses. Uncertainties quoted on water-sample cation concentrations and $^{87}Sr/^{86}Sr$ ratios, corrected for cyclic inputs, include analytical uncertainties of 5 percent (1σ) combined with the propagated uncertainties on the rainfall and hotspring inputs. The average fraction of cations derived from rain and hot-spring inputs for all the Alaknanda tributary and mainstem analyses ranges from 27 percent for Na, 10 percent for K, 8 percent for Ca, 3 percent for Mg and 8 percent for Sr. In the Marsyandi and tributaries the average rain and hot-spring derived fractions are 27 percent for Na, 14 percent for K to less than 4 percent for Ca, Mg, Si and Sr. The root-mean square difference between uncorrected and corrected $^{87}Sr/^{86}Sr$ ratios is 0.0024 in the Alaknanda dataset and 0.0015 in the Marsyandi data set. In the Marsyandi the relatively radiogenic hot spring inputs are more significant in the September dataset than in the May dataset and most significant in the mainstem data from below Chame. The relatively large scatter within the Alaknanda hot-spring data set ($^{87}Sr/^{86}Sr$ = 0.766 ± 0.021, 1σ) imparts a significant average uncertainty of ~0.00023 on the corrected water $^{87}Sr/^{86}Sr$ ratios. The less radiogenic Sr-isotopic composition of the hot spring at Chame (0.73793) was used to correct the Marsyandi mainstem samples collected at and below Chame. All elemental ratios are quoted as molar ratios except Sr/cation ratios that are quoted as nmol/μmol (denoted $Sr^{\#}/Ca$).

The main approaches to apportioning dissolved constituents in rivers and ground-water to their respective carbonate and silicate mineral sources are: 1) stoichiometric assignment of the dissolved constituents to their source mineral phases (modal decomposition: for example Garrels and Mckenzie, 1967; Drever, 1997; Price and others, 2008) and 2) use of characteristic element ratios of the carbonate and silicate inputs (for example Négrel and others, 1993; Harris and others, 1998; Krishnaswami and Singh, 1998; Singh and others, 1998; Gaillardet and others, 1999; Galy and France-Lanord, 1999; Bickle and others, 2003, 2005). For the second method the elemental ratios of the carbonate and silicate end-members used in the calculations are variously taken from analyses of average rocks (for example Gaillardet and others, 1999), bedrocks to catchments (Bickle and others, 2003), riverine bed and/or sus-pended loads, determined from the water composition of small monolithological catchments or extrapolated from the composition arrays of the water analyses (for example Négrel and others, 1993; Singh and others, 1998; Bickle and others, 2005).

All the methods have significant limitations and we explore these further in this paper. Modal decomposition of waters given the source mineral compositions has been used most successfully to model chemical weathering in soil chronosequences (for example White and others, 2008). Blum and others (1998) used this method to investigate mineral weathering in the Raikhot watershed in High Himalayan Crystal-line Series on Nanga Parbat. However the limited number of dissolved components that are derived from stoichiometric constituents of minerals significantly restricts the number of minerals which can be considered in the calculations. Further, components which may be hosted on exchangeable sites on minerals are generally not included in the modeling and trace-element concentrations (for example Sr) in the source minerals are generally unknown. One major advantage of such calculations is that information is recovered on the weathering rates of the different minerals (for example Maher and others, 2009).

Use of element ratios of the carbonate and silicate bedrock components assumes that within the two end-members the constituent carbonate or silicate minerals dissolve at the same rate. Within the carbonate component, calcite dissolves signifi-cantly faster than dolomite. The silicate component contains more complex mineralo-gies and, although K-feldspar, plagioclase, biotite and hornblende exhibit similar far-from-equilibrium dissolution rates, the actual rates depend on the hydraulic characteristics which control the mineral-fluid chemical exchange at the pore-scale and the dependence of the reaction rates on the approach to thermodynamic equilibrium (White and Brantley, 2003). Consequently mineral dissolution rates exhibit large differences in the few well-studied soil profiles (for example Maher and others, 2009). Incongruent dissolution of phases with precipitation of secondary phases including carbonates and clay minerals is difficult to incorporate in the modeling. Indeed, in Himalayan settings it is probable that precipitation of secondary calcite removes a large fraction of the Ca from the waters (for example Galy and others, 1999; Jacobson and others, 2002; Oliver and others, 2003; Bickle and others, 2005). This means that methods of estimating the silicate- and carbonate-derive Sr fluxes based on Sr/Ca ratios of the carbonate and silicate sources underestimate Sr fluxes in certain catchments by a factor of two (for example Krishnaswami and others, 1999; Galy and others, 1999; English and others, 2000). In the Himalayas the high $^{87}Sr/^{86}Sr$ ratios of carbonates that result from metamorphic exchange with silicate minerals (Bickle and others, 2001) preclude simple use of the $^{87}Sr/^{86}Sr$ ratios to discriminate carbonate and silicate Sr inputs.

River waters commonly form arrays in composition space which probably result from mixing of two or more components. Methods that infer the characteristic

element ratios of the carbonate and silicate inputs from such arrays of water composi-
tions are designed to allow for the incongruent dissolution of the end-members (for
example Négrel and others, 1993; Singh and others, 1998; and Bickle and others,
2005). However we show below that these arrays may arise from mixing of waters from
different sources with differing extents of incongruent dissolution and that this may
rotate the arrays and cause large errors in the estimate of the composition of the
silicate input.

In this paper we evaluate the water chemistry in terms of source rock compositions
and mineralogy determined by analyses of bedloads. We first discuss the Marsyandi
catchment in Nepal, because the time-series sampling in conjunction with analyses of
the bedloads, demonstrates that the Sr-Ca-Na-(Mg) trends used by Bickle and others
(2005) are perturbed by a systematic relationship between the amount of secondary
carbonate precipitation and the fraction of silicate component in the waters. The
magnitude of secondary carbonate precipitation is critical to apportioning the fraction
of the riverine cations derived from carbonate and silicate source. This is followed by a
review of 1) use of subsets of Sr-Ca-Mg-Na-K-^{87}Sr/^{86}Sr compositions of waters and
bedloads to estimate the magnitude of precipitation of secondary calcite in the
Marsyandi and Alaknanda Tethyan Sedimentary Series catchments and attribution of
the cations to carbonate or silicate sources, 2) comparison of this approach with
modeling dissolution and precipitation of minerals, including secondary calcite, in the
system Ca-Mg-Na-K-Al-Si, and 3) a comparison of the modeling in Sr-Ca-Mg-Na-K-
^{87}Sr/^{86}Sr space and of mineral modes with the constraints imposed by the stable Ca
and Mg isotopic compositions presented by Tipper and others (2006b). The discussion
of the Tibetan Sedimentary Series catchments is followed by a similar review of the
High Himalayan Crystalline Series and Lesser Himalayan Series catchments in the
Alaknanda.

micas whereas bed and suspended loads in the Ganges flood plain also show the

It follows that there are many factors which may complicate deconvolution of the
chemical inputs to waters to their source components. One set of factors is inherent to
the methods themselves, notably incongruent dissolution and precipitation reactions
during weathering and the potential behavior of cations on exchangeable sites on
minerals. Another set of factors relate to our ability to characterize the compositions of
both the waters and source rocks. Potential factors include 1) heterogeneity of bedrock
and bedrock erosion rates, 2) spatial or temporal decoupling of chemical weathering
and physical erosion within catchments so that the sampled bedload is not characteris-
tic of the source of the dissolved chemical flux, 3) temporal variations in the sources of
the dissolved flux and 4) secular changes in physical and chemical erosion rates such
that outputs from catchments are out of equilibrium. Spatial and short time-scale
heterogeneities in catchment bedrock and erosion rates and sources of the dissolved
flux can be revealed by sub-sampling bedload and water chemistry within the catch-
ment and by time-series sampling of water outputs from the catchment.

In this paper we evaluate the water chemistry in terms of source rock compositions
and mineralogy determined by analyses of bedloads. We first discuss the Marsyandi
catchment in Nepal, because the time-series sampling in conjunction with analyses of
the bedloads, demonstrates that the Sr-Ca-Na-(Mg) trends used by Bickle and others
(2005) are perturbed by a systematic relationship between the amount of secondary
carbonate precipitation and the fraction of silicate component in the waters. The
magnitude of secondary carbonate precipitation is critical to apportioning the fraction
of the riverine cations derived from carbonate and silicate source. This is followed by a
review of 1) use of subsets of Sr-Ca-Mg-Na-K-^{87}Sr/^{86}Sr compositions of waters and
bedloads to estimate the magnitude of precipitation of secondary calcite in the
Marsyandi and Alaknanda Tethyan Sedimentary Series catchments and attribution of
the cations to carbonate or silicate sources, 2) comparison of this approach with
modeling dissolution and precipitation of minerals, including secondary calcite, in the
system Ca-Mg-Na-K-Al-Si, and 3) a comparison of the modeling in Sr-Ca-Mg-Na-K-
^{87}Sr/^{86}Sr space and of mineral modes with the constraints imposed by the stable Ca
and Mg isotopic compositions presented by Tipper and others (2006b). The discussion
of the Tibetan Sedimentary Series catchments is followed by a similar review of the
High Himalayan Crystalline Series and Lesser Himalayan Series catchments in the
Alaknanda.

The results emphasize the significance of secondary carbonate precipitation and
the importance of secular variations in chemical weathering inputs. They also reveal
the complexity of the controls on riverine water chemistries imposed by source rock
mineralogies, incongruent dissolution and precipitation reactions and the possible
exchange reactions with clay minerals.

<div style="text-align:center">BEDLOAD AS A REPRESENTATIVE SAMPLE OF BED ROCK</div>

Bedload samples provide the best average of catchment bedrock although compo-
sitions may be biased by dissolution of minerals, variable erosion rates within catch-
ments and are subject to hydrodynamic sorting. Lupker and others (2012) show that
the composition of bed and suspended loads from Himalayan mountain rivers are
primarily controlled by mixing between quartz and feldspathic minerals and detrital
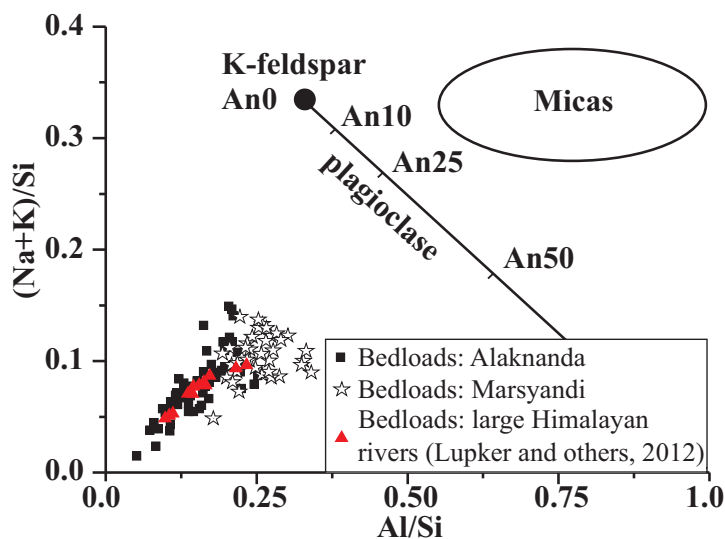micas whereas bed and suspended loads in the Ganges flood plain also show the

Fig. 3. Bedloads from the Alaknanda and Marsyandi catchments compared to bedloads from large rivers in the Himalayas from Lupker and others (2012). Note trend lies between quartz and mixtures of plagioclase and/or micas. Alaknanda catchment bedloads at high (Na+K)/Si and Al/Si are from tributaries draining the calc-silicate Deoban Formation, at low (Na+K)/Si but high Al/Si from small High Himalayan catchments and the low (Na+K)/Si and Al/Si samples are from quartzite-dominated catchments. Alaknanda samples are from the HHCS and LHS and Marsyandi samples are mainly from the TSS (supplementary data table S2, http://earth.geology.yale.edu/~ajs/SupplementaryData/2015/01BickleTables.pdf).

influence of secondary minerals. The low fractions of soluble silicate dissolved in the mountains (<1%, West and others, 2002) means that the silicate fractions of the bedload differ little from their source rocks in the more rapidly eroding catchments.

The silicate fractions of bedloads from the Alaknanda and Marsyandi catchments show limited dispersion (fig. 3) mainly attributable to lithological heterogeneity and sedimentary sorting. Comparison of bulk bedload compositions, bedload leach and residue compositions in Sr-Ca-Na space (figs. 4 and 5) shows that the scatter of bedloads primarily reflects mixtures of carbonate and silicate end-members. Particularly important for correct apportionment of Sr to carbonate and silicate sources is the factor-of-six scatter in the Sr/Ca ratios of the carbonate fraction. Also apparent from this diagram (and see fig. 5B) is the generally elevated Sr/Ca ratio of the waters compared with the source rocks. It is clear from figure 4 that calculating the distribution of Sr between silicate and carbonate sources using average compositions of the source rocks will have order-of-magnitude uncertainties. In this paper we therefore make the calculations for individual catchments using the composition of the silicate and carbonate components in the bedload of the catchment.

TIBETAN SEDIMENTARY SERIES CATCHMENTS: WATER CHEMISTRY

Waters from the Marsyandi and Alaknanda Tethyan Sedimentary Series catchments are similar to those draining the other catchments dominated by the Tethyan Sedimentary Series (Galy and France-Lanord, 1999; English and others, 2000). They contain high dissolved solids (TDS 100–500 mg/l), have relatively high sulphate concentrations (upto ~1500 μmol/L) and are characterized by Sr/Ca ratios up to four times higher than bedrock. The high sulphate concentrations contribute to between 27 percent and 47 percent of the anion charge and are a consequence of sulphide oxidation (Galy and France-Lanord, 1999; Turchyn and others, 2013).
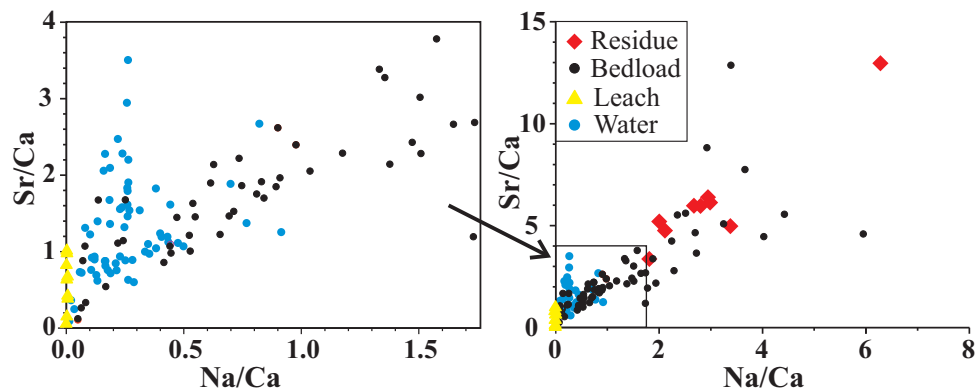
Fig. 4. Sr/Ca versus Na/Ca compositions of bedloads, their corresponding water samples and acetic acid leaches and residues from leaching of bed-load samples for the Alaknanda catchment (tables S1, S2 and S3 in supplementary data, http://earth.geology.yale.edu/~ajs/SupplementaryData/2015/01BickleTables.pdf). Left-hand figure magnifies samples with lower Sr/Ca and Na/Ca. Note scatter in bedload and particularly wide range of Sr/Ca ratios of acetic acid leaches of carbonate fractions. Three bed-load samples (AK182, AK251 and AK264) plot outside the area of the figure.

Modeling of Marsyandi Water and Bed-load Compositions in Sr-Ca-Na Space

The Marsyandi waters exhibit correlations in element ratio plots such as Sr/Ca versus Na/Ca comparable with the bedloads (fig. 5). Bickle and others (2005) presumed that such correlations represented variable mixtures between two distinct components derived from carbonate and silicate sources. It was assumed that the best-fit line must pass through these 'end-members', albeit with their Sr/Ca and Na/Ca ratios changed from the rock values by incongruent reactions such as precipitation of secondary calcite. It was shown that the fractions of carbonate and silicate-derived Sr, calculated from the inferred carbonate and silicate Sr/Ca ratios, are relatively insensitive to the choice of silicate Ca/Na ratio and concluded that between 50 and 70 percent of the Sr was derived from silicate sources. This fraction is unusually high for a carbonate-dominated catchment, a consequence of the fits which implied silicate $1000Sr/Ca$ (henceforth 1000Sr written $Sr^{\#}$) ratios ~60 and $Sr^{\#}/Na$ ratios ~16 at Na/Ca = 4, which are much higher than those of most silicate rocks (the silicate residues reported below have high $Sr^{\#}/Ca$ of 40 to 80 but at much higher Na/Ca of 40–100). Below we show that the time-series samples from the Marsyandi mainstem at the exit from the Tethyan Sedimentary Series exhibit well-correlated cation ratios consistent with inputs of two components with differing ratios of silicate- to carbonate-derived cations (for example figs. 5 and 6). However a correlation between the seasonal variations in the ratio of silicate to carbonate inputs and the amount of secondary carbonate precipitation rotates the correlation line in Sr/Ca-Na/Ca space such that the gradient is steeper than that of the bedload array. This causes over-estimation of the silicate Sr inputs by modeling the water Sr-Ca-Na compositions on the basis of end-member compositions inferred from the correlation through the water compositions.

The Marsyandi mainstem sampled over the period June 2002 to August 2003 (Tipper and others, 2006a) exhibits a much smaller range of compositions than the tributaries but a tighter correlation between Sr/Ca and Na/Ca (fig. 5). Tipper and others showed that the water compositions exhibited seasonal variations attributed to variable mixing of a carbonate-dominated rapid runoff with more silicate-dominated deeper circulating groundwaters. Andermann and others (2012) have emphasized the
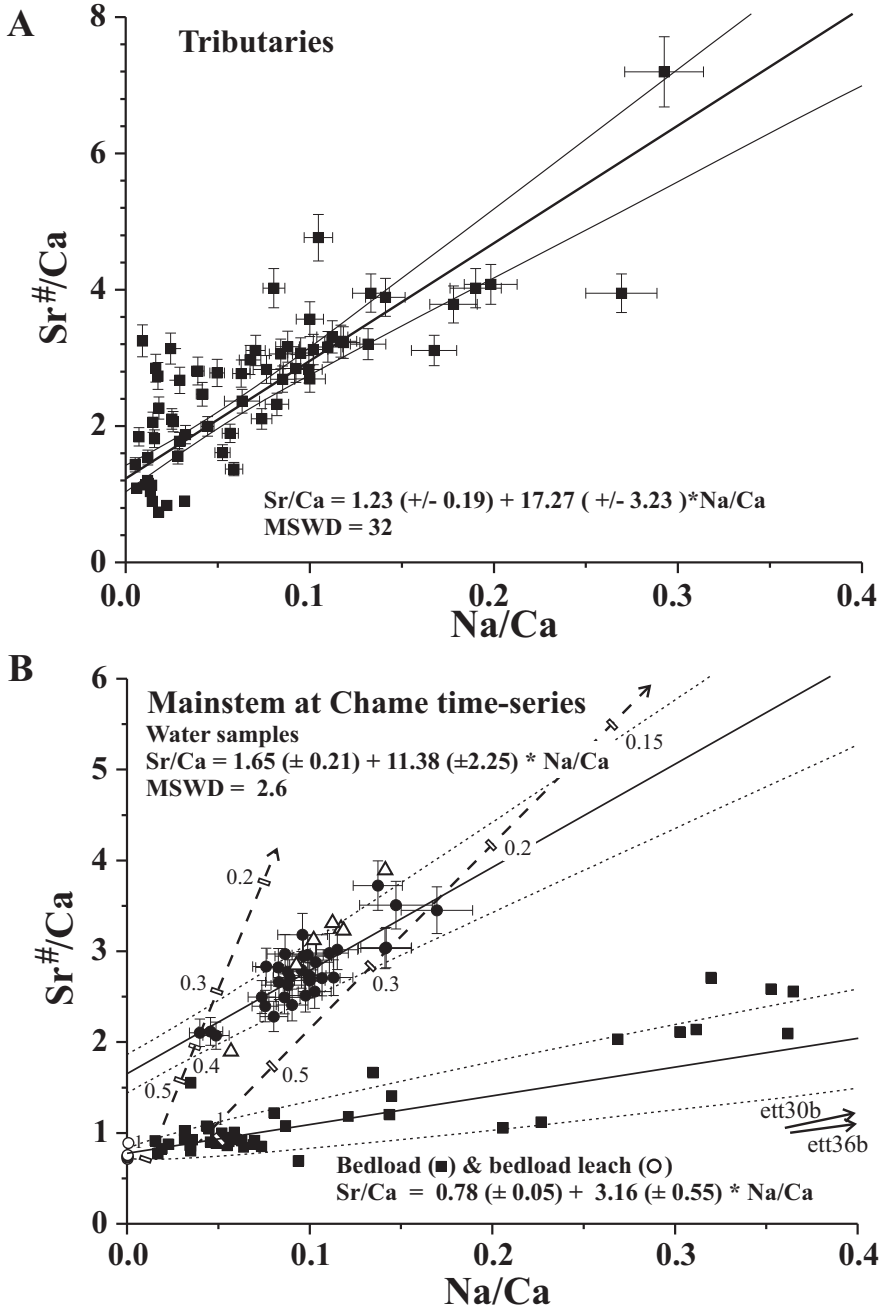
Fig. 5. (A) Sr#/Ca (mmol/mol) versus Na/Ca molar ratio correlation diagrams for water samples from May and September 2002 Marsyandi tributary sample sets. Line fit and 1σ uncertainties (dotted lines) as described by Bickle and others (2005). Error bars (not shown where smaller than symbols) are for 1σ and represent the combined uncertainties from the analyses and corrections for rain and hot-spring inputs. (B) Sr#/Ca (mmol/mol) versus Na/Ca molar ratio for time-series water samples from Marsyandi below Chame (circles with error bars) compared to bed-load (solid squares), and bed-load leaches (open circles). Open triangles are water samples from Marsyandi at and above Manang and Khangsar Khola. Best fits and 1σ error bounds (dotted lines) shown. 2 bed-load samples plot outside diagram. Dashed lines are trajectories showing loci of samples precipitating secondary calcite, assuming K_D Sr:Ca = 0.05 (Rimstidt and others, 1998) for initial Na/Ca ratios of 0.015 and 0.04. Values are fraction of initial Ca remaining in water (γ).
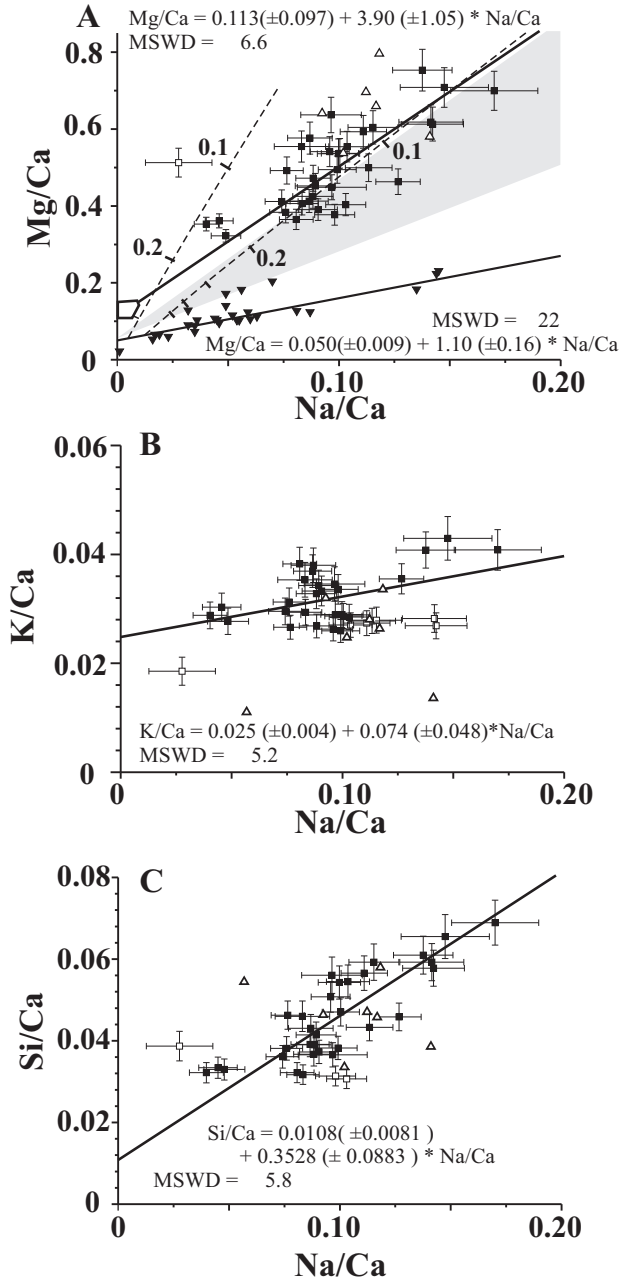
Fig. 6. (A) Mg/Ca, (B) K/Ca, and (C) Si/Ca variation with Na/Ca for time series-water samples from the Marsyandi below Chame. Regressions and 1σ errors calculated as in Bickle and others (2005). Open triangles are water samples from Marsyandi at and above Manang and the Khangsar Khola and are not included in regressions. Solid squares with error bars are rain and spring corrected water compositions. Solid triangles are bedload samples from Marsyandi catchment (7 samples lie outside plot). On figure 6A dashed lines are trajectories for precipitation of secondary calcite with values of initial Ca remaining in water (γ) shown. Shaded region on figure 6A shows loci of source carbonate-silicate correlations calculated from mineral modal proportions—see text.

significance of variable groundwater inputs to Himalayan catchments. The mainstem Ca/Na varies between 7 and 36, compared with the tributaries that range from 3.4 to 195. This is to be expected as the mainstem is a flux-weighted average of the tributaries. The correlation between Sr/Ca and Na/Ca exhibits a scatter only marginally in excess of that expected from the estimated compositional uncertainties (Mean Squared Weighted Deviates, MSWD = 2.6, fig. 5B) and Mg/Ca, Si/Ca and K/Ca exhibit similar small scatter (fig. 6). The data fit a hyperplane in Sr-Ca-Na-Mg space within analytical error (MSWD = 0.8, fitting routines described by Bickle and others, 2005). This suggests that much of the scatter on the tributary composition arrays arises from geological controls, either variability of source rock composition or differing reaction progress for the incongruent dissolution or precipitation reactions that govern the water chemistry.

The coherence of the mainstem trends suggests that 1) the water compositions are dominated by two-component mixing, 2) the range of rock cation compositions does not vary systematically across the catchment, and 3) that the extents of incongruent dissolution or precipitation reactions do not vary over the catchment such as to obscure the two-component mixing trends. This implies that the role of changes in weathering reactions due to factors such as rock type, altitude or catchment type (for example glaciated or ice-free) are much less important in defining river-water compositions than variations in the relative contributions of the carbonate and silicate components and the progress of catchment-wide dissolution and precipitation reactions.

Displacement of Water Compositions from Bedload Array

The cause of the marked difference between the source (bedload, leach and residues) and the water Sr/Ca ratios (figs. 4–6) is critical to understanding the chemical weathering processes. This must reflect incongruent dissolution or precipitation reactions. High Sr might result from dissolution of high-Sr minerals such as strontianite, aragonite, celestite or apatite (for example Muller, 1969), incongruent leaching of Sr from minerals or precipitation of phases with low Sr contents during weathering reactions. The coherent correlation of high Sr/Ca ratios of the waters across indices of varying carbonate to silicate input makes it unlikely that the high Sr/Ca reflects input from a single high Sr mineral. Similarly if the high Sr/Ca ratios of the waters arises from enhanced leaching of Sr from minerals this must take place during leaching of both the carbonate as well as the silicate phases. McGillen and Fairchild (2005) show that the Sr/Ca of initial leach fractions of calcite may be enriched up to a factor of 8 but only when <1 percent of the calcite is dissolved. The fraction of calcite weathered in the Marsyandi Tibetan Sedimentary Series catchment is constrained to be between about 3 and 20 percent based on estimates of rainfall and measurements of the river water flux at Chame (see Tipper ms, 2006 and table 4 below).

An alternative and favored mechanism for elevation of water Sr/Ca ratios is precipitation of secondary carbonate (Galy and others, 1999; English and others, 2000; Jacobson and others, 2002; Bickle and others, 2005). Four observations support this hypothesis: 1) Secondary carbonate has low Sr/Ca ratios compared with either primary biogenic carbonates or silicate minerals and is widely observed in High Himalayan catchments (English and others, 2000; Tipper and others, 2006b, 2008). 2) The Marsyandi waters exhibit Ca-isotope compositions systematically heavier than the mixing array between their source Tethyan Sedimentary Series limestones and silicates and the sign of this enrichment is consistent with precipitation of the fraction of secondary calcite required to explain water Sr/Ca ratios (Tipper and others, 2006b). 3) Mg/Ca ratios in the waters are also elevated compared with bed-load compositions (fig. 6A). Modal calculations in the system Si-Al-Mg-Ca-K-Na, discussed below, imply

precipitation of significant amounts of low Sr and Mg calcite. 4) We show below that mass-balance of the Mg-isotopic compositions presented by Tipper and others (2006b) requires dissolution of Mg-calcites to be balanced by precipitation of a lower Mg secondary calcite combined with a significant input of Mg from silicate phases, as also discussed below. We therefore explore the hypothesis that Ca loss to secondary calcite is responsible for the discrepancy between the water compositions and bed-load/rock array. We investigate the consistency of the calculations in subsets of Sr-Ca-Mg-Na-K-$^{87}Sr/^{86}Sr$ space.

Calculation of the Magnitude of Secondary Calcite Precipitation

The magnitude of secondary calcite fractionation may be calculated from the displacement of samples from the bed-load array in Sr-Ca-Na space as illustrated on figure 5B. This calculation assumes that dissolution of the silicate and carbonate minerals in the bedload is congruent for Sr, Ca and Na, that precipitated calcite does not subsequently exchange with waters (Rayleigh fractionation) and that the Sr/Ca molar partition coefficient, k_d^{Sr}, is small. The change in Sr/Ca ratio with calcite fractionation is given by (for example Albarède, 1995)

$$Sr\,/\,Ca = Sr\,/\,Ca|_0 \gamma^{(k_d^{Sr}-1)} \tag{1}$$

where $Sr/Ca|_0$ is the Sr/Ca molar ratio of the water prior to secondary calcite precipitation and γ is the fraction of original Ca remaining in the water. The magnitude of secondary calcite precipitation $(1-\gamma)$ may then be calculated as that needed to return the sample to the bed-load array defined by the least-squares best fit to the bedload samples:

$$Sr\,/\,Ca = A + BNa\,/\,Ca \tag{2}$$

where A and B are the intercept and slope of the bedload array, (fig. 5B). γ is given by the solution of the equation

$$0 = Sr\,/\,Ca\gamma^{(1-k_d^{Sr})} - A - B\gamma Na\,/\,Ca \tag{3}$$

where the Sr/Ca and Na/Ca are the measured molar ratios in the water.

The equilibrium Sr/Ca molar calcite-water partition coefficient, k_d^{Sr}, is of the order 0.025 but the effective partition coefficient increases with the rate of calcite precipitation to ~0.2 (for example Tesoriero and Pankow, 1996; Rimstidt and others, 1998; Gabitov and Watson, 2006; Nehrke and others, 2007; Nielsen and others, 2013; Thein and others, 2014). In this paper we take $k_d^{Sr} = 0.05$ but the calculated Ca loss to secondary calcite $(1-\gamma)$ is insensitive to the value of the partition coefficient while it remains small.

Seasonal Dependence of Secondary Calcite Precipitation

The magnitude of secondary calcite precipitation calculated for the Marsyandi time-series samples at Koto from equation 3 correlates with water Ca/Na (fig. 7B). The waters with lowest Na/Ca ratio of ~0.04 have γ values of ~0.37, that is loss of about 60 percent of the initial Ca to secondary calcite. The waters with the highest Na/Ca ratio of ~0.17 have γ values of ~0.23 implying a loss of ~75 percent of the initial Ca. It is this correlation, with the more silicate-rich waters precipitating proportionally more Ca into secondary calcite that rotates the water array on the Sr/Ca to Na/Ca diagrams. The rotation invalidates simple extrapolation of the correlation to define the carbonate and silicate end-members, as used by Singh and others (1998) and Bickle and others (2005). A plot of γ against time shows a seasonal control with the fraction of secondary carbonate deposition increasing in the dry season (γ decreasing) (fig. 7A).
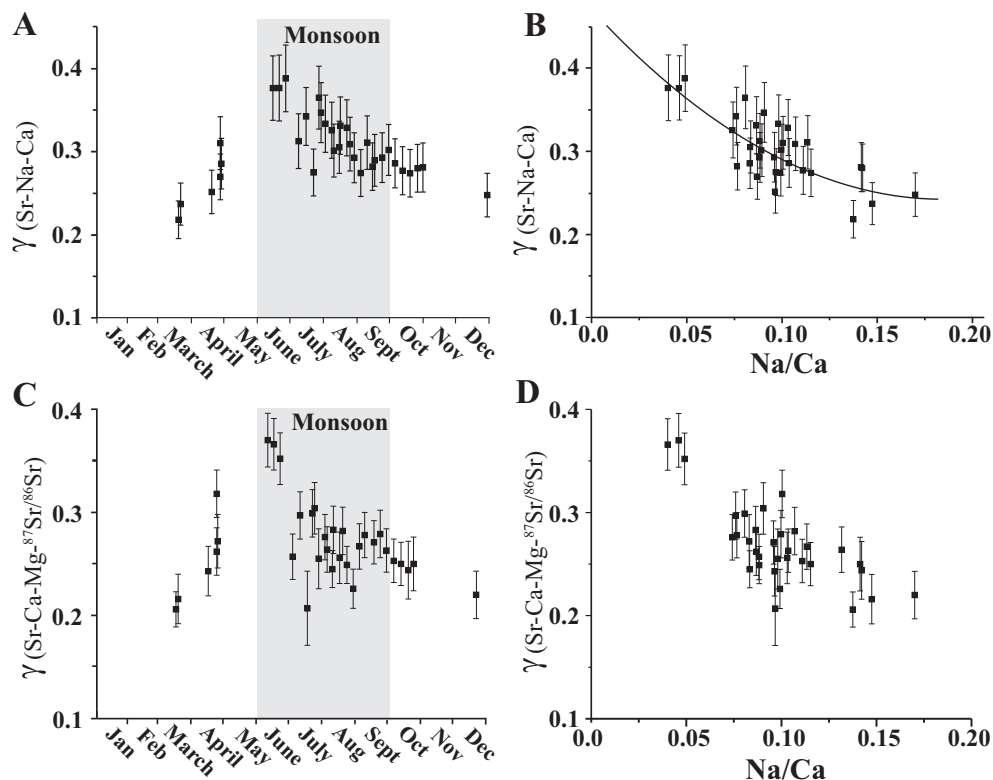
Fig. 7. Secondary calcite precipitation from Marsyandi time-series samples. Figure 7A shows fraction of Ca remaining (γ) calculated from transposition of water samples to rock and bed-load array in Sr-Ca-Na space (see fig. 5B) and figure 7C γ calculated in Sr-Ca- Mg-^{87}Sr/^{86}Sr space (see below). Errors 1σ. Figure 7B shows fraction of Ca remaining after Ca loss to secondary calcite (γ) calculated in Sr-Na-Ca space as a function of water Na/Ca (uncorrected for Ca loss), a proxy for the fraction of silicate Ca input. Line is best-fit hyperbola appropriate for two-component mixing. Figure 7D shows γ as a function of water Na/Ca calculated in Sr-Ca- Mg-^{87}Sr/^{86}Sr space.

Tipper and others (2006a) noted that the relative inputs from silicate and carbonate end-members, characterized by Si/Ca and ^{87}Sr/^{86}Sr ratios, showed a strong seasonal variation with higher silicate inputs during the drier seasons and high carbonate inputs during the monsoon. The Marsyandi Tethyan Sedimentary Series catchment is large and exhibits systematic variations in metamorphic grade and rock units as illustrated by the scatter in ^{87}Sr/^{86}Sr ratios plotted against Ca/Na (fig. 8). However Tipper and others (2006a) concluded that the apparent increase of carbonate inputs during the monsoon was not simply due to seasonal variations in the location of chemical weathering yields.

The seasonal variations were attributed to a greater contribution of rapid runoff during the monsoon, which rapidly saturated with carbonate, compared with a greater contribution of deeper groundwaters during the drier seasons where their longer residence times facilitated more weathering of silicate minerals. Hydrological modeling of Nepalese catchments by Andermann and others (2012) show that between ~15 and 55 percent of discharge is from groundwater sources with residence times of a month or more.

The correlation of the magnitude of secondary calcite precipitation with the seasonal changes in precipitation and the fraction of silicate to carbonate weathering
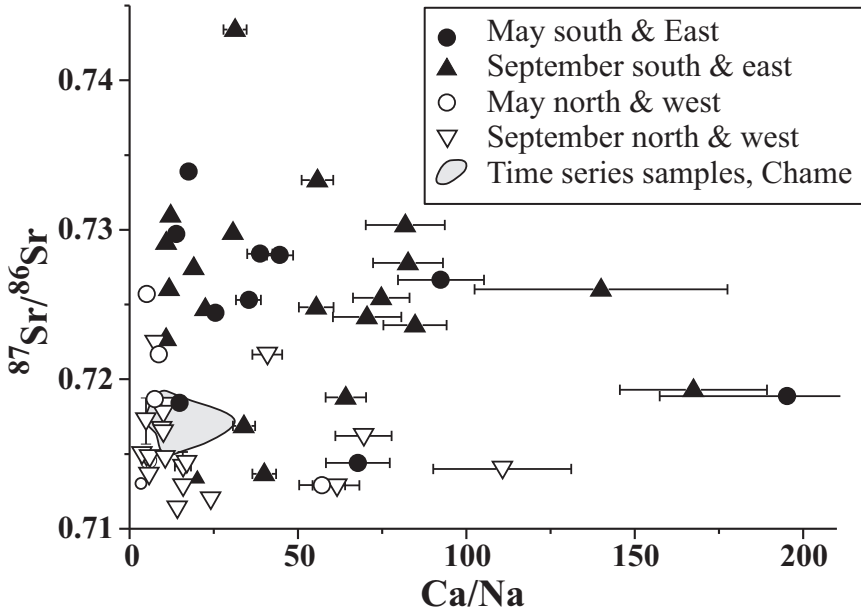
Fig. 8. $^{87}Sr/^{86}Sr$ ratios of Tethyan Sedimentary Series tributaries to the Marsyandi collected in May and September, divided into areas draining younger rocks in the north and west from those draining older rocks in the south of the Marsyandi east of Manang (fig. 2). Shaded area shows range of mainstem time-series sample set from Marsyandi below Chame.

(fig. 7) is consistent with the calcite precipitation being driven by increased aridity, freezing, and possibly the pH increase consequent on dissolution of silicate minerals (Knauss and others, 2005).

Estimates of Secondary Carbonate and Carbonate- and Silicate-Derived Sr, Ca and Mg in Multi-Component Space

The calculations above consider only the components Sr-Ca-Na. Mg/Ca and K/Ca ratios should also be elevated by precipitation of secondary calcite whereas $^{87}Sr/^{86}Sr$ ratios will remain unchanged. It is also important to calculate the fractions of Sr, Ca and Mg derived from weathering of carbonate and silicate sources. Here calculation of the magnitude of precipitation of secondary calcite and the elemental inputs from carbonate and silicate sources is based on the assumption that the acid leaches characterize the carbonate component in the bedload, and the residue from leaching, the silicate component. This assumption, that the cation ratios of the silicate chemical weathering component are similar to those of bed-load silicate fraction, could be problematic. K is retained in micas and K/Ca ratios of the waters are much less than the K/Ca ratios of the silicate bedload. The consequences of this are apparent in the calculations using K/Ca ratios below. The relative weathering rates of Sr, Ca, Na and Mg will depend on the silicate mineralogy as various combinations of these elements exhibit mutual solid-solution in different minerals. For example where plagioclase is a dominant mineral, Sr, Ca and Na release will likely be congruent. In the low-grade bedrocks of the Marsyandi Tibetan Sedimentary Series catchment these elements appear to be distributed between plagioclase, partially weathered biotite, chlorite, muscovite and clay minerals. A test of the extent of incongruent release of the soluble elements is a comparison of the calculated fractions of carbonate and silicate weathered in subsets of Sr-Ca-Na-Mg-K-$^{87}Sr/^{86}Sr$ space.
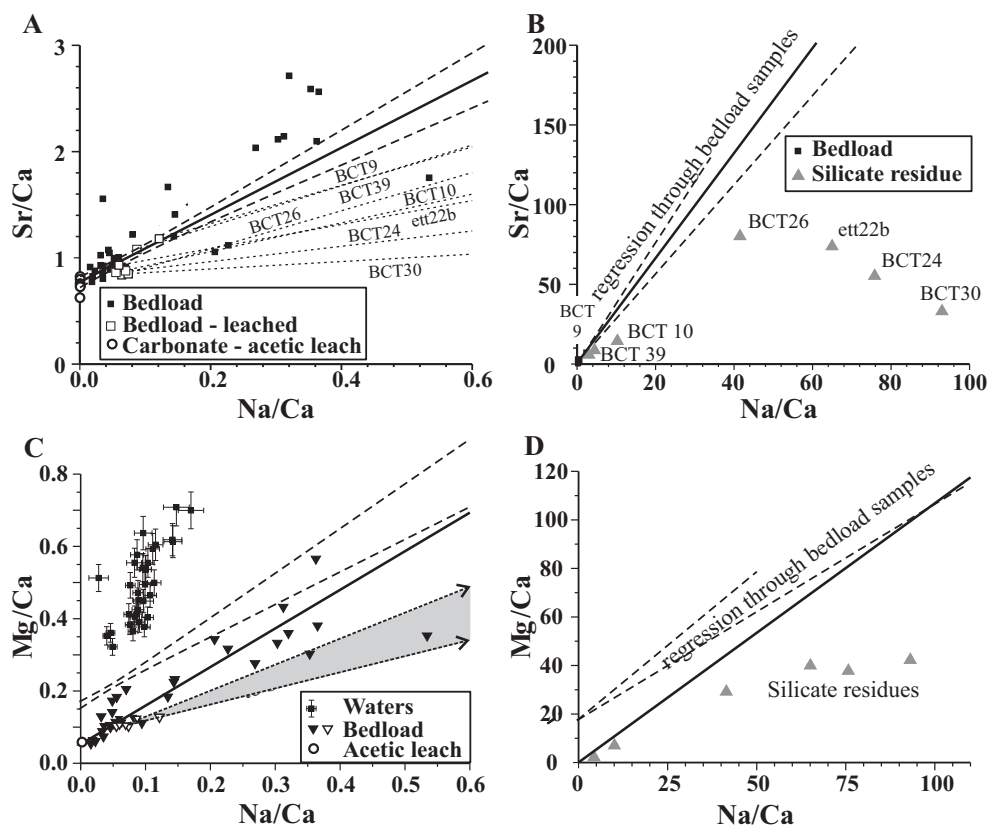
Fig. 9. (A) Sr/Ca versus Na/Ca for acetic acid leaches (open circles) and whole bed-load samples from the Marsyandi Tibetan Sedimentary Series catchment (fig. 2). Open squares are bed-load samples subject to leaching (supplementary data table S3, http://earth.geology.yale.edu/~ajs/SupplementaryData/2015/01BickleTables.pdf). Solid line is regression through whole bedload samples and dashed lines ±1σ error bounds. Bedload samples subject to leaching shown as open squares. Dotted lines connect bedload compositions to their respective silicate residue compositions which plot at much higher Sr/Ca and Na/Ca. (B) Silicate residues and bed-load regression with whole bedloads plotting close to origin. Note that the high Na/Ca silicate residues, BCT 22, 26, 30 and ett22b are from the upper Marsyandi, lower grade, catchments. The lower Na/Ca residues, BCT9 (the Nar) and BCT10 (the Marsyandi) are at the exit of the Tibetan Sedimentary Series catchments. BCT39 was collected 3 km downstream from BCT10 where inputs of higher grade rocks including Ca-bearing plagioclase result in more normal silicate Na/Ca ratios (3 to 10). (C) Mg/Ca versus Na/Ca for Marsyandi waters, bedload and regression through bedload samples with 1σ error bands, and average acetic acid leach. Open triangles are the mainstem bedload samples for which leach and residue analyses are given in supplementary data table S3. Shaded area delimits loci of vectors towards silicate residues shown in figure 9D. (D) Mg/Ca versus Na/Ca for bedload silicate residues against regression through bedload samples.

Figure 9 illustrates the compositions of the bulk bedloads, their acetic acid leaches and silicate residues on plots of Sr/Ca and Mg/Ca versus Na/Ca. The acetic acid leaches from the Marsyandi catchment are all very similar with $Sr^{\#}/Ca$ ratios between 0.625 and 0.825, Mg/Ca ratios between 0.041 to 0.053 and Na/Ca ratios between 2×10^{-4} and 5×10^{-4} (table S3). The silicate residues exhibit a much greater scatter with the samples from the upper Marsyandi catchment (BCT24, 26, 30 and ett22b) exhibiting very high Sr/Ca, Mg/Ca and Na/Ca ratios. Many of the residues have Sr/Ca ratios well below the array of bed-load samples at comparable Na/Ca ratios, which might reflect systematic variations in the compositions of the carbonate and silicate

end-members. By contrast, the residues Mg/Ca ratios scatter only just below the array defined by the bed-load samples in the Mg/Ca-Na/Ca space.

The method of calculation of the fractions of cations derived from silicate and carbonate sources is equivalent to use of the characteristic element ratios of these sources (for example, Negrel and others, 1993; Gaillardet and others, 1999; Bickle and others, 2005) with addition of the calculation of Ca loss to secondary calcite. The weight fractions of the carbonate and silicate sources (F_{crb} and F_{sil}, kg/L) added to a liter of water to give the water composition are modeled by solving two or more of the simultaneous mass-balance equations. These relate the concentration of cation, 'i', in the water, X^i_{Cwat} (mmole/L), to the sum of the weight of the carbonate component input (F_{crb}, kg/L), concentration of cation 'i', X^i_{crb} (mmol/kg), and weight fraction of the silicate component input (F_{sil}, kg/L), concentration of cation 'i', X^i_{sil} (mmol/kg),

$$X^i_{Cwat} = F_{crb}.X^i_{crb} + F_{sil}.X^i_{sil} \ . \tag{4}$$

The water composition, X^i_{Cwat} in equation 4, is that unmodified by precipitation of secondary calcite. The observed water compositions, X^i_{wat}, may be related to the inputs by correcting equation 4 for secondary calcite precipitation (with γ as defined above) as

$$X^i_{wat} = (F_{crb}.X^i_{crb} + F_{sil}.X^i_{sil}).\gamma^{k^i_d} \tag{5}$$

where k^i_d is the solid-fluid molar partition coefficient for the cation 'i', relative to Ca. In the calculations below we take ($k^{Ca}_d = 1$, k^{Sr}_d and $k^{Mg}_d \sim 0.05$ and k^{Na}_d and $k^K_d = 0$).

Mass-balance of $^{87}Sr/^{86}Sr$ can be expressed as a simple mixing equation as secondary calcite precipitation does not alter Sr-isotope ratios giving

$$^{87}Sr/^{86}Sr_{wat} = \frac{(^{87}Sr/^{86}Sr_{crb}.F_{crb}.X^{Sr}_{crb} + \ ^{87}Sr/^{86}Sr_{sil}.F_{sil}.X^{Sr}_{sil})}{(F_{crb}.X^{Sr}_{crb} + F_{sil}.X^{Sr}_{sil})}. \tag{6}$$

The concentrations of the components input from the carbonate and silicate sources (X^i_{crb}, X^i_{sil}) are taken from the concentrations in the bed-load leach and silicate residue (note it is only ratios of these concentrations that determine the relative partition between silicate and carbonate sources). The solution of these equations assumes that elements dissolve congruently within the carbonate end-member and the silicate end-member but that the carbonate and silicate end-members may dissolve at different rates. The three unknowns F_{crb}, F_{sil} and γ are determined by solution of equations 5 and 6 for three or more of the soluble cations (Na, K, Ca, Mg, Sr, $^{87}Sr/^{86}Sr$). Here we solve equations 5 and 6 by a Marquart-Levenberg minimization (Press and others, 1986) of a chi-squared (χ^2) variable defined as

$$\chi^2 = \sum_{i=1}^{n} \frac{(X^i_{wat} - X^i_{calc})^2}{\sigma^2_i} \tag{7}$$

where X^i_{calc} is the estimated water composition calculated by the right hand side of equations 5 or 6, σ^2_i is the 1σ variance of water compositions and the values of F_{crb}, F_{sil} and γ are sought which minimize χ^2 for the set of n soluble elements chosen. Uncertainties on F_{crb}, F_{sil} and γ were calculated based on the uncertainties in the water compositions corrected for rain and spring inputs where necessary increased to give the χ^2 value appropriate to the degrees of freedom (Bevington and Robinson, 1992, eq 6.17). The errors calculated by the Marquart-Levenberg minimization program of Press and others (1986) were checked against a Monte Carlo routine. Including an additional 5 percent 1σ uncertainty on the element concentrations in the carbonate

leach and 15 percent 1σ uncertainty on the element concentrations in the residue only increased the uncertainty on the silicate fraction (F_{sil}) by a factor of two and on the carbonate fraction (F_{crb}) and γ by a factor of 1.5. It should be noted that the calculated uncertainties do not include the systematic errors, probably dominated by incongruent dissolution, discussed further below and these systematic differences are more significant.

An exact solution of equations 5 and 6 is possible if only three soluble elements are used and the data can be illustrated on ratio-ratio diagrams such as figure 5. It is not easy to graphically portray solutions for subsets of 4 or more elements in two dimensions although subsets of three of the four or more elements may be shown. Instead we use χ^2 as a measure of the quality of the fit and compare the observed and calculated values of soluble elements or isotopes for those elements used in the solution. The predicted concentrations or Sr-isotopic ratios of the parameters not used in the solution of equations 5 or 6 are also calculated from the estimates of the magnitudes of the carbonate and silicate components, F_{crb}, F_{sil}, and the compositions of the carbonate and silicate components taken as the bed-load leach and residue compositions (for example table 2). These results are used to calculate the percentages of Sr, Mg and Ca derived from silicate and carbonate sources.

In the system Sr-Ca-Na the solution of equations 5 and 6 is equivalent to first calculating the fraction of initial Ca (γ) remaining in a water sample after loss of secondary calcite by the transposition necessary to return each water sample to the rock/bed-load array (or leach-silicate residue array) in Sr/Ca to Na/Ca space (fig. 5B), and secondly calculating the fractions of Sr, Ca and Na derived from the silicate and carbonate components given an estimate of their Na/Ca ratios (Bickle and others, 2005, fig. 2 and equations 2 to 4). Bickle and others showed that the solutions are very insensitive to the poorly constrained Na/Ca ratios of the silicate component. The solutions show similar insensitivity to the choice of silicate residue composition (table 2).

Marsyandi time-series samples below Chame.—Solutions to equations 5 and 6 for subsets of the soluble elements and $^{87}Sr/^{86}Sr$ ratio are listed in table 2. This gives the average, maximum and minimum quality of fit (χ^2), average γ and the average fractions of the silicate and carbonate components and their average standard deviations for the time-series set of 33 samples from Koto. The bed-load sample BCT10 collected at Chame, 2 km upstream of Koto where the time series samples were collected, is taken as representative of bedrock to the catchment. The BCT10 leach (acetic acid leach plus silicate-corrected HCl leach—see supplementary data table S3, http://earth.geology.yale.edu/~ajs/SupplementaryData/2015/01BickleTables.pdf) is taken as representative of the carbonate input and its residue as representative of the silicate inputs.

The solutions reveal substantial differences in the apportioning of cations to silicate and carbonate sources in Sr-Ca-Na, Sr-Ca-K and Sr-Ca-Mg-$^{87}Sr/^{86}Sr$ spaces. For Sr-Ca-Na this gives a mean γ of 0.23 (range 0.16 to 0.29, fig. 7A, table 2) and implies that about 0.2 percent of the Ca, 5 percent of the Sr and 20 percent of the Mg are derived from the silicate source. The fit for Sr-Ca-K gives a similar range of γ's (mean 0.22) but implies only 1 percent of the Sr and 5 percent of the Mg are derived from silicate phases, a result of K being preferentially retained in muscovite in the bedload, with the additional potential for non-conservative behavior relating to uptake in vegetation. Fits for Sr-Ca-Na-$^{87}Sr/^{86}Sr$ (and Sr-Ca-Na-K not shown) scatter considerably in excess of the estimated errors in the water compositions (χ^2 for one degree of freedom equals 60 and 86 respectively; note that a fit with one degree of freedom, appropriate for calculating three parameters from four equations, gives $\chi^2 = 1$ if the data scatter as expected for the estimated uncertainties). Calculation of the water $^{87}Sr/^{86}Sr$ ratios

TABLE 2

Averages of regressions for Marsyandi time-series samples against leach and residues compared to compositions of waters (μmol/L except Sr nmol/L)

Elements in regression	χ² mean	χ² min	χ² max	γ (1σ)	F_{sil} (1σ)	F_{crb} (1σ)	Sr	Ca	Mg	Na	K	$^{87}Sr/^{86}Sr$	%Sr sil (1σ)	%Mg sil (1σ)	%Ca sil (1σ)
Water*							2372	851	433	86	27	0.71709			
Sr-Ca-Mg-$^{87}Sr/^{86}Sr$	0.4	0.0	2.6	0.28 / 0.04	1.93 / 0.14	0.90 / 0.06	2358	850	432	411	637	0.71759	22.8 / 2.0	61.0 / 2.7	1.3 / 0.4
Sr-Ca-Mg-$^{87}Sr/^{86}Sr$ Corrected**	0.8	0.0	5.2	0.27 / 0.02	1.31 / 0.11	0.74 / 0.05	2403	851	425	306	440	0.71729	21.1 / 2.0	59.0 / 3.0	1.1 / 0.3
Sr-Ca-Mg-$^{87}Sr/^{86}Sr$ Silicate-HCl+res***	1.2	0.0	6.0	0.27 / 0.03	1.61 / 0.12	0.92 / 0.07	2353	851	453	343	546	0.71707	21.5 / 2.0	70.7 / 2.5	3.2 / 0.8
Sr-Ca-Na****				0.23 / 0.02	0.39 / 0.04	1.12 / 0.06			257		132	0.71440	4.6 / 0.5	20.7 / 1.9	0.20 / 0.02
Sr-Ca-Na-$^{87}Sr/^{86}Sr$	73	67	256	0.35 / 0.33	0.44 / 0.14	0.99 / 0.43	2130	853	241	95	148	0.71485	7.1 / 4.8	27.8 / 13.6	0.34 / 0.26
Sr-Ca-K				0.22 / 0.02	0.07 / 0.01	1.17 / 0.06			220	16		0.71375	0.9 / 0.1	4.7 / 0.4	0.04 / 0.004
Sr-Ca-Mg-$^{87}Sr/^{86}Sr$ against BCT26	1.8	0.0	6.4	0.49 / 0.06	2.14 / 0.14	0.66 / 0.07	2296	851	442	516	801	0.71691	41.4 / 3.1	78.5 / 2.2	0.69 / 0.09
Sr-Ca-Mg-$^{87}Sr/^{86}Sr$ against BCT30	0.9	0.0	4.4	0.28 / 0.03	2.39 / 0.19	0.58 / 0.03	2343	851	435	590	676	0.71704	8.3 / 0.8	56.7 / 2.6	0.20 / 0.05

Averages of results of regressing individual Marsyandi time-series suite of water samples corrected for cyclic inputs (Tipper and others, 2006a, table 2, excluding sample MT25) against BCT10 acetic leach plus silicate-corrected HCl leach for carbonate component and BCT10 residue except where noted. Note that 1σ errors on γ, F_{sil} and F_{crb} are the average of the errors of the 33 individual samples of the time-series set. Values for γ, F_{sil} and F_{crb} and fractions of Sr, Mg and Ca derived from silicates exhibit marked seasonal variations (figs. 7 and 10).

  * Water is the average composition of the time-series water samples. The values given for each regression are from the best fit (where only three elements are regressed an exact fit is obtained to those elements).

  ** BCT10 Leach and residues corrected for loss by weathering as in table 3.

  *** Against BCT10 carbonate from acetic leach, silicate from residue plus HCl leach.

  **** Regression with three parameters gives exact solution.

from fits in Sr-Ca-Na and Sr-Ca-K space predict water $^{87}Sr/^{86}Sr$ ratios ~0.714 against the measured average value of ~0.718. The discrepancies might arise from preferential loss of ^{87}Sr from damaged Rb-sites in the silicates although this would conflict with the consistency of the calculations in Sr-Ca-Mg-$^{87}Sr/^{86}Sr$ space. Alternatively Na may be preferentially retained on exchangeable sites on clay minerals but this would require about 75 percent of the Na to be lost to match the Sr-isotope values.

By contrast, solutions to Sr-Ca-Mg-$^{87}Sr/^{86}Sr$ fit with a mean χ^2 of 0.4 and the maximum χ^2 equal to 2.6, indicating fits to the four variables within the estimated uncertainties. This system implies slightly higher values for γ (mean 0.28, range 0.22 to 0.37) and significantly higher fractions of Ca, Sr and Mg derived from silicate sources (~1.3%, 21% and 60%). The solutions exhibit the same time-dependence with γ highest in the monsoon (compare figs. 7A and 7C) but with more significant decreases in the fractions of silicate-derived Sr and Mg during the monsoon (fig. 10).

Systematic uncertainties, in addition to incongruent dissolution, that might affect these results include 1) the Mg content of the carbonate being estimated by combining the acetic leach with the silicate-corrected HCl leach which might be a poor approximation for weathering of mixed calcite-dolomite carbonate fractions, 2) heterogeneity of bedloads and 3) the bedload silicate residues may have lost a significant fraction of their soluble elements during the weathering.

For the Marsyandi Tibetan Sedimentary Series samples which contain minimal dolomite, use of the composition of the acetic leach instead of the combined acetic and silicate-corrected HCl leach as the carbonate component makes no significant difference. The maximum potential effects of sample heterogeneity may be assessed by using the range of bedloads sampled. For example if the Marsyandi time-series samples are regressed for Sr-Ca-Mg-$^{87}Sr/^{86}Sr$ using the leach-residues of upper Marsyandi sample BCT26 or the Khangsar Khola sample BCT30, the two most extreme samples from the catchment (fig. 9), the quality of the fits is similar (mean $\chi^2 = 1.8$), but there are some differences in both estimates of γ and the fractions of cations derived from silicate (table 2). However calculations of F_{crb}, F_{sil} and γ from these bed-load samples using the water compositions from the upper Marsyandi give results indistinguishable from bed-load and time-series water samples from Chame (compare table 2 and table 3).

It is possible to make estimates of the fractions of cations removed from the silicate and carbonate components of the bedload (table 4). The regressions discussed above combined with the discharge data give the dissolved fluxes. Estimates of the physical erosion rate combined with the bed-load compositions give the fluxes of solid carbonate and silicate materials. The silicate- and carbonate-derived dissolved cation fluxes are calculated by averaging the water compositions weighted by the calculated silicate and carbonate fractions for each time-series sample by month (and interpolating for the unsampled months) and by the monthly water fluxes at Koto given by Wolff-Boenisch and others (2009). The fluxes in table 4 include the estimated fractions of Ca, Mg and Sr deposited in secondary calcite. The silicate residue flux is calculated from the composition of the BCT10 residue from leaching (table S3) and the total particulate load estimated by Gabet and others (2008) from suspended load measurements and the assumption that bedload is 50 percent of suspended load. This implies erosion rates of 1.0 ± 0.3 mm/yr, consistent with the 1.2 ± 0.2 mm/yr (2σ error) erosion rate inferred from cosmogenic isotope analyses in the comparable Tibetan Sedimentary Series catchment in the Alaknanda by Vance and others (2003). The bed-load sample BCT10 contains 36 weight percent carbonate.

The results (table 4) show that a maximum of between 2 and 29 percent of the soluble major cations are removed from the silicate fraction of these rather depleted second-cycle metasediments. The fractions of Ca, Mg and Sr removed are consistent
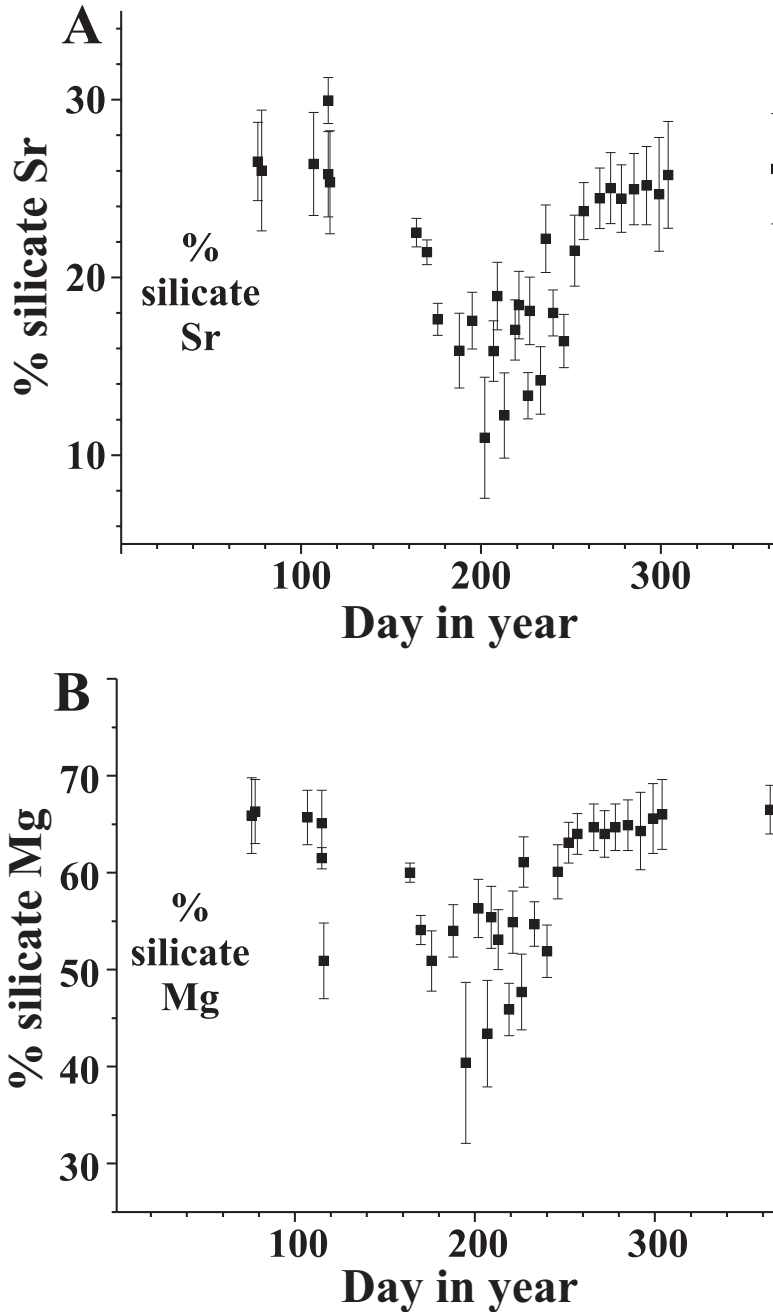
Fig. 10. Temporal variation of fraction of Sr (A) and Mg (B) derived from silicate for Marsyandi time-series samples calculated in Sr-Ca-Mg- ^{87}Sr/^{86}Sr space.

at ~29 percent and, surprisingly, a higher fraction (but of a much lower flux) than the ~20 percent of the carbonate dissolved. Because Ca-Mg-Sr are lost to weathering in equal proportions repeating the regression of the Koto time-series samples against

TABLE 3

Regressions for Upper Marsyandi, Nar and Alaknanda Tethyan Sedimentary Series catchments compared to compositions of waters (μmol/L except Sr nmol/L)

Elements in regression	χ^2 mean	χ^2 min	χ^2 max	γ 1σ	F_{sil} 1σ	F_{crb} 1σ	Sr wat calc	Ca wat calc	Mg wat calc	Na wat calc	K wat calc	$^{87}Sr/^{86}Sr$ wat calc	%Sr sil	%Mg sil	%Ca sil
Sr-Ca-Mg-^{87}Sr/^{86}Sr	1.3	0.2	3.4	0.29	3.92	1.16	4018	1173	719	141	26	0.71746	21.7	67.2	0.35
Upper Mars*				0.02	0.19	0.06	4086	1173	707	903	1232	0.71747	0.07	0.9	0.01
Sr-Ca-Na**				0.23	0.61	1.41	4018	1173	719	141	26	0.71746	3.6	20.8	0.045
Upper Mars*				0.02	0.04	0.08			357		206	0.71323	1.9	4.2	0.004
Sr-Ca-Mg-^{87}Sr/^{86}Sr	25	3.9	46	0.22	1.6	1.7	4039	1143	676	142	26	0.71432	20.6	42.0	2.2
Nar***				0.08	0.6	0.4	4604	1143	535	531	580	0.71458	7.2	10.4	1.0
Sr-Ca-Na**				0.21	0.42	1.8	4039	1143	676	142	26	0.71432	6.3	16.2	0.6
Nar***				0.02	0.03	0.1			374		165	0.71297	0.5	1.2	0.1
Sr-Ca-Na-^{87}Sr/^{86}Sr	3.1	0.3	7.4	0.25	0.44	1.2	2326	638	473	124	26	0.71911	5.8	10.5	0.40
Alaknanda****				0.03	0.05	0.07	2302	638	472	69	183	0.71910	0.7	1.3	0.05
Sr-Ca-Na**				0.24	0.80	1.15	2326	638	473	124	26	0.71911	9.8	17.0	0.69
Alaknanda****				0.02	0.05	0.07			495		325	0.72073	0.8	1.3	0.06
Sr-Ca-Mg-Na-^{87}Sr/^{86}Sr	20	5.3	31	0.23	0.56	1.27	2326	638	473	124	26	0.71911	6.8	12.1	0.21
Alaknanda****				0.06	0.13	0.20	2465	633	509	87	229	0.71947	1.3	2.2	0.09

* Average of samples from upper Marsyandi catchment sampled at or above Manang (ett22, CT20, CT24, CT26 regressed against bedload BCT26 sampled at these localities using HAc+silicate-corrected HCl for carbonate and residue for silicate).

** Regression with three parameters gives exact solution, and exact match for the three elements fitted so only the water element concentration given for fitted elements.

*** Average of Nar time-series samples against BCT9 using HAc + silicate-corrected HCl for carbonate and residue for silicate.

**** Average of samples AK95, AK109, AK261 from Alaknanda Tethyan Sedimentary Series catchment (Dhauli Ganga) collected at or close to Chamoli against bedload AK95RS using HAc for carbonate and residue for silicate.

<div align="center">Table 4</div>

Chemical flux estimates in dissolved, particulate, and carbonate and silicate particulate fractions in Marsyandi at Koto and % of silicate dissolved for Marsyandi bedload samples based on modeling in Sr-Ca-Mg-^{87}Sr/^{86}Sr space

	Dissolved flux*	Dissolved silicate flux*	Dissolved carbonate flux*	Particulate flux including carbonate**	Particulate silicate Flux (residue from leaching)	Particulate carbonate flux (acetic acid + silicate-corrected HCl leach)	% of silicate cations dissolved*	% of carbonate cations dissolved*
	Water flux = 6.2x10⁸ m³/yr			Particulate flux = 2.2x10⁹ kg/yr				
	------------------------------------ 10⁶ mol/yr ------------------------------------							
Na	47	47		510	466		9	
K	16	16		1110	720		2	
Ca	1922	18	1904	9206	45	7582	29	20
Mg	244	133	111	944	328	426	29	21
Sr	1.45	0.26	1.18	8.8	0.67	4.8	28	20

 * Ca, Mg and Sr include fraction precipitated in secondary calcite.
 ** Particulate flux calculated from analysis of whole bedload, discrepancy with sum of carbonate from leach and silicate from residue reflects loss in leaching process.

BCT10 leach and residue corrected for the weathering loss gives nearly identical values for the precipitation of secondary calcite and the fractions of Sr, Mg and Ca derived from silicate and carbonate (table 2).

The incongruent dissolution implied by table 4, where the fractions of Na and K lost from the silicate are significantly less than the fractions of Ca, Mg and Sr explains the discrepancies in the regressions involving Na and K with Sr-Ca-Mg-^{87}Sr/^{86}Sr. The overestimates in water Na and K fluxes in the regressions of Sr-Ca-Mg-^{87}Sr/^{86}Sr in tables 3 and 4 arise because smaller fractions of the alkalis, and particularly K, are lost from the silicate residues than Sr, Ca, or Mg. K is probably retained because muscovite (or illite), a major detrital mineral in the bedload, weathers slowly (Drever, 1994). Na may also be retained in micas or on exchangeable sites on clay minerals. It should be noted that Lupker and others (2012) observed that greater fractions of Na and K than Ca and Mg were lost from silicate minerals in the Ganges flood plain.

Upper Marsyandi, Nar and Alaknanda Tethyan Sedimentary Series catchments.—Table 3 lists regressions for the upper Marsyandi catchments and the Nar and Alaknanda (Dhauli Ganga) Tethyan Sedimentary Series catchment. Again, regression of Sr-Ca-Mg-^{87}Sr/^{86}Sr for the Nar and Upper Marsyandi samples gives reasonable fits whereas regression in Sr-Ca-Na implies significant discrepancies in ^{87}Sr/^{86}Sr budgets. The Sr-Ca-Mg-^{87}Sr/^{86}Sr regressions imply much higher water Na and K concentrations than measured and the fractions of silicate Sr and Mg for the Nar and upper Marsyandi are within error of those for the time-series samples below Chame. Regression in Sr-Ca-Na implies much lower fractions of silicate Sr and Mg. The carbonate fraction from the bed-load sample from the Alaknanda (Dhauli Ganga) Tethyan Sedimentary Series catchment, AK95RS, has significant dolomite (Mg/Ca acetic leach = 0.16, acetic plus HCl silicate-corrected = 0.21). However the silicate residue is similar to that of BCT10. Regression of the water samples from the Tibetan Sedimentary Series catchment in the upper Alaknanda (Dhauli Ganga) against carbonate and silicate fractions of AK95RS gives similar values for γ and the fractions of silicate Sr and Mg for fits in Sr-Ca-Mg-^{87}Sr/^{86}Sr, Sr-Ca-Na and Sr-Ca-Mg-Na-^{87}Sr/^{86}Sr spaces. The fractions of silicate-

derived Sr and Mg (~7% of Sr and 17% of Mg) are significantly smaller than in the Marsyandi (tables 2 and 3). Unlike the Marsyandi and Nar catchments, the calculated water Na concentrations are less than the observed values. By contrast the calculated K concentrations are much higher than observed as for the Marsyandi and Nar catchments. Again, the calculated fraction of secondary calcite precipitation decreases during the early monsoon (see fig. 11F below).

MODELING WEATHERING REACTIONS USING DETRITAL MINERAL COMPOSITIONS IN THE MARSYANDI CATCHMENT

It is instructive to compare the results of modeling inputs using the bulk chemical and isotopic compositions of carbonate and silicate bedload with calculation of the fractions of the source minerals weathered by modal decomposition of the water chemistry. Detrital mineral compositions were determined by electron micro-probe analyses of minerals in the bedloads.

Table S4 in the supplementary data (http://earth.geology.yale.edu/~ajs/SupplementaryData/2015/01BickleTables.pdf) lists the average compositions of detrital silicate and carbonate minerals out of ~700 analyses of grains in mounts of bed-load samples, BCT10 from the Marsyandi at Chame, BCT26 from the Marsyandi above the confluence with the Khangsar Khola which drains the low-grade terrain to the northwest, BCT36 from the Khangsar Khola which drains part of the northern flanks of Annapurna range and BCT9 from the Nar at its confluence with the Marsyandi. The bedloads contain large fractions of carbonate minerals and grain mounts containing sufficient silicate minerals were obtained by removing the carbonate fraction through leaching with cold 1 M HCl or 1M acetic acid. Averages of mineral compositions from leached and unleached mounts were indistinguishable. The silicate minerals analyzed are primarily quartz (6%), muscovite (55%), biotite (19%), vermiculite (4%), chlorite (8%), with minor hematite or Fe-oxyhydroxides (6%), trace K-feldspar and plagioclase (3 grains of albite, 1 grain An55%), garnet, epidote, clinopyroxene, tremolite, rutile, titanite, ilmenite, magnetite, Cr-spinel and kaolinite. Note that the silicate minerals were selected by reconnaissance EDS electron- micro-probe analysis with apparent quartz and calcite excluded and feldspar and mica minerals preferentially sought for analysis. However as optical identification of minerals in the grain mounts is challenging, the numbers analyzed should only be considered an approximate guide to their abundance. The carbonates are predominantly calcite (mean Mg 1.7 mol %, and only 8 analyses greater than 4 mole % Mg) with only two dolomite grains in the 170 carbonates analyzed. The Mg content of the calcites is significantly lower than that of the respective acetic acid leaches (4 mol% Mg) and may preferentially include secondary calcite or the leaches may have removed some Mg from the silicates. The Mg/Ca ratio of the Al-silicate corrected HCl leaches ranges from 0.8 to 1.5 and ratio of Ca in the HCl leach to that in the acetic leach indicates that the HCl leach may reflect ~2 percent mol fraction dolomite in the bedload. The biotites exhibit markedly low K contents (1.0 ± 0.5, 1σ, versus the ideal 2 per 22 oxygen formula unit) and probably comprise oxy- or hydro-biotites or interlayered chlorite-biotite or vermiculite-biotite. Biotite-like compositions on the basis of Si, Al, and Fe+Mg with K < 0.7 per 22 oxygen formula unit were classified as vermiculite.

Mineral Modes Dissolved as Calculated from Water Compositions

The modes of minerals consumed or precipitated during fluid-rock reactions may be calculated from the water composition provided that the number of chemical components available is equal or greater than the number of minerals and given the assumption that minerals dissolve congruently (see Drever, 1997, chapter 12).

The modes of primary carbonate, plagioclase, biotite/chlorite consumed and secondary calcite, kaolinite and smectite precipitated are solved from the six mass-
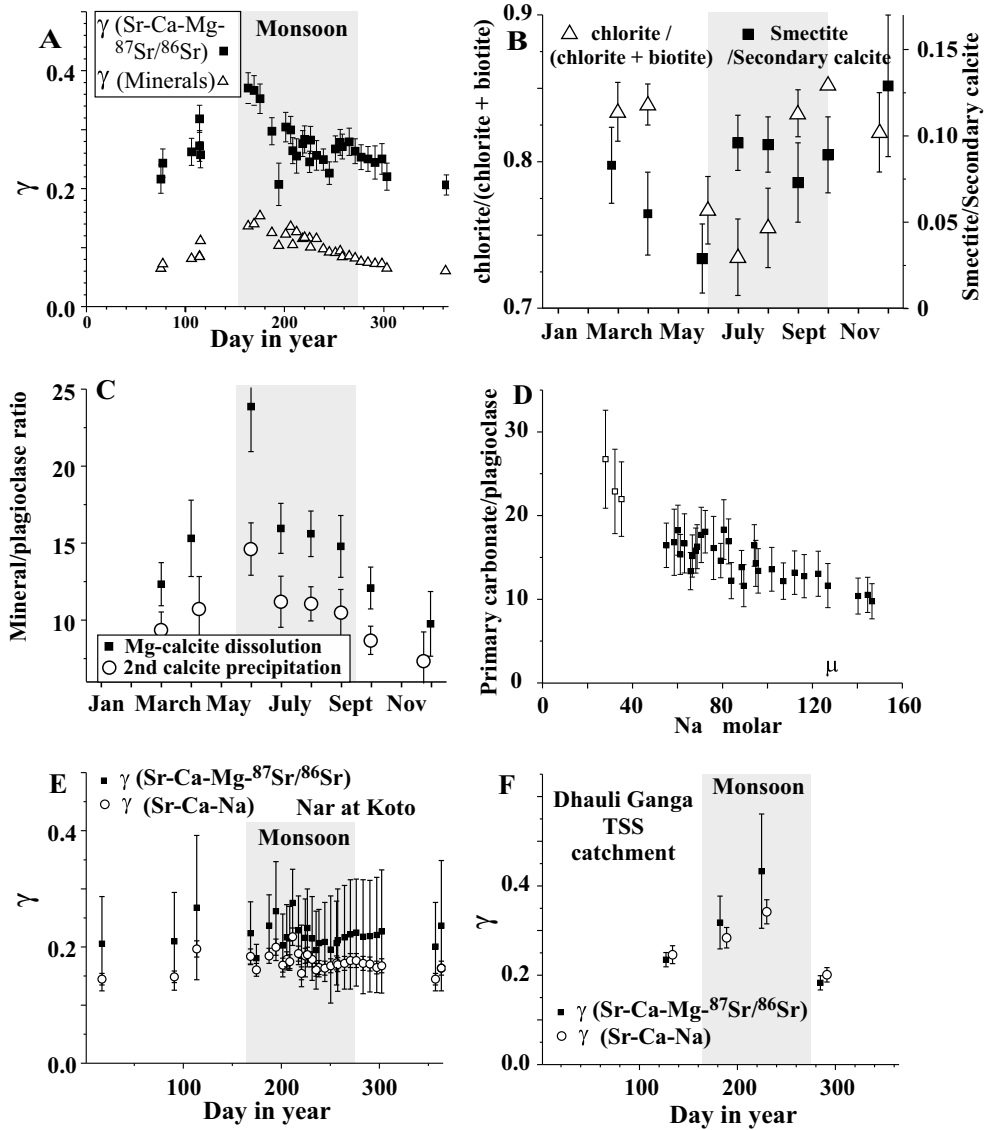
Fig. 11. Secondary calcite and calculated mineral modes for the Marsyandi catchment (A to D) compared with the Nar and Alaknanda Tethyan Sedimentary Series catchments (E, F). Figure 12A compares γ (the fraction of Ca remaining after precipitation of secondary calcite) calculated from the mineral modes compared to regression in Sr-Ca-Mg-^{87}Sr/^{86}Sr. Figures 12B, 12C, and 12D all calculated with the chlorite-biotite ratio adjusted to match γ calculated in Sr-Ca-Mg-^{87}Sr/^{86}Sr space. Figure 12B shows the ratio of smectite to secondary calcite (right-hand axis) and estimated ratio of chlorite to total chlorite plus biotite (left-hand axis). (C) Ratio of dissolution of primary Mg-bearing carbonate and precipitation of secondary calcite relative to plagioclase dissolution with the expected increase in the relative dissolution of carbonate during the monsoon. Figure 12D shows the ratio of primary carbonate dissolved to plagioclase plotted against water Na content, dilution of which is an inverse proxy for discharge. Note that the June samples, shown with open symbols in figures 12D lack Cl analyses and their corrections for cyclic inputs are less certain. In figure 12E the Nar shows comparable fractions of secondary calcite precipitation calculated from regressions in Sr-Ca-Na and Sr-Ca-Mg-^{87}Sr/^{86}Sr space but limited seasonal trends. Figure 11F shows seasonal increase in γ in Alaknanda Tethyan Sedimentary Series catchment. In figures 11E and F, γ calculated in Sr-Ca-Mg-^{87}Sr/^{86}Sr space (solid squares) is only marginally higher than that in Sr-Ca-Na space (open circles).

Table 5

Average mineral compositions used for modal decomposition of Marsyandi catchments

Element	Biotite*	Chlorite*	Primary calcite*	Secondary calcite**	Kaolinite***	Smectite****
Si	2.58	2.69			2.00	3.55
Al	2.37	2.61			2.00	1.88
Mg	0.84	1.51	0.053	0.013		0.37
Ca	0.01	0.04	0.944	0.987		0.10
Na	0.04	0.01				0.04
K	0.67	0.02			0.01	0.16

* From table S4.
** Calculated average composition with $K_d^{Sr} = 0.05$ and precipitation to give average water Sr/Ca
*** From Melo and others (2001).
**** From Drief and Nieto (2000).

balance equations for the components SiO_2-Al_2O_3-MgO-CaO-Na_2O-K_2O in the water, given that the water contains negligible Al_2O_3. With the number of mineral phases equal to the number of equations, the uncertainties calculated on the mineral modes only reflect the estimated uncertainties in the water compositions, corrected for rain and hot-spring inputs. The most problematic aspect is the choice of mineral phases in geologically complex catchments. In Himalayan environments, secondary silicate mineral precipitation occurs predominantly as kaolinite and to a more limited extent as smectite. The principle minerals in the source rocks include quartz, calcite, plagioclase, K-feldspar, biotite, muscovite and chlorite with clay minerals in lower grade rocks and a range of less common silicate minerals. Since modes of only six minerals may be constrained by the water compositions, it is necessary to make some simplifying assumptions. Quartz weathers extremely slowly and is ignored. K-feldspar weathers more slowly than plagioclase and modes calculated with plagioclase-K-feldspar-biotite-calcite-Mg calcite-kaolinite invariably involve amounts of K-feldspar within error of zero, so that K-feldspar is excluded. Similarly muscovite weathers relatively slowly and is ignored. The primary carbonate dissolved in the Marsyandi catchment will be some mixture of Mg-bearing calcite and the very rare dolomite. Mass-balance then requires significant precipitation of a low-Mg calcite. Thus six minerals are initially considered: Mg-carbonate, low Mg calcite, plagioclase, biotite, kaolinite and smectite. Further complications not considered here include: 1) that plagioclase comprises albite-anorthite solid solutions (anorthite may weather more rapidly than albite), 2) the Mg-calcite component may include dolomite as well as calcite which also weather at different rates and 3) biotites and smectites may exhibit a range of compositions with smectites containing cations in exchangeable as well as in structural sites.

To reduce the system to a solvable set of equations we initially assume that 1) the Mg-carbonate has the Mg/Ca ratio of the combined acetic and silicate-corrected HCl leach, 2) the plagioclase dissolution is stoichiometric and has the Ca/Na ratio of the silicate residue from bed-load leaching, 3) biotite has the average composition analyzed (table 5), 4) smectite has a single composition including exchangeable ions taken from an average of the continental samples of Drief and Nieto (2000) (table 5) and 5) the secondary calcite has an average Mg content of 1.7 mol percent appropriate to a calcite-water Mg/Ca partition coefficient of 0.05 and precipitation of 75 percent of the Ca, as indicated by the Sr-Ca-Mg-^{87}Sr/^{86}Sr systematics. This Mg concentration lies within the range of Himalayan travertines analyzed by Tipper and others (2006b).

The results, calculated using a least-squares routine (fig. 12A), imply very large amounts of Mg-calcite dissolution and calcite re-precipitation greater than that indi-
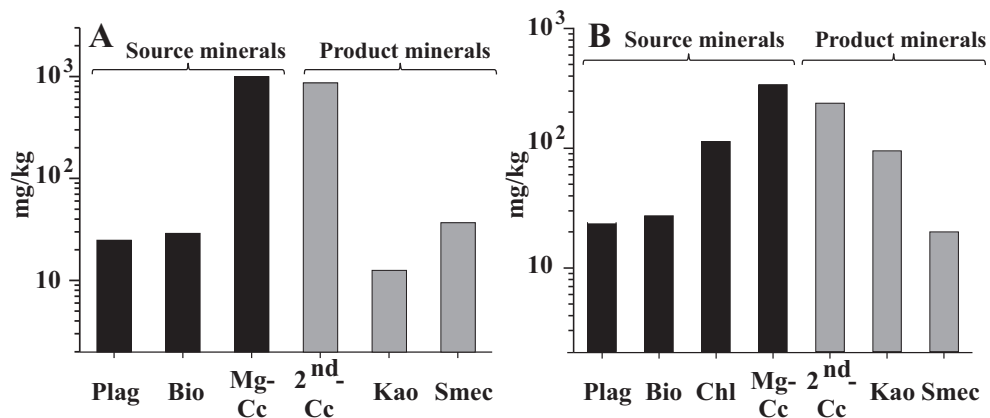
Fig. 12. Water-flux weighted average mineral modes consumed or precipitated in mg of mineral per kg of water (on Log_{10} scale) for Marsyandi time-series samples sampled at Koto. (A) Results modeled with biotite as the only significant Mg-bearing silicate mineral. This implies dissolution and re-precipitation of large amounts of carbonate. Figure 12B calculated to give the same fraction of Ca reprecipitated as secondary calcite as in the calculations based on the Sr-Ca-Mg-^{87}Sr system by including chlorite and adjusting the chlorite to biotite ratio. The average uncertainties in modal proportions arising from the uncertainties in the concentrations of the components in the waters are about 6% in (A) and range between ~1% (kaolinite) to 28% (smectite) in (B). The major uncertainties arise from the uncertainties on the type and composition of the source minerals. Plag = plagioclase, Bio = biotite, Chl = chlorite, Mg-Cc = primary Mg-bearing carbonate, 2nd-Cc = secondary calcite, Kao = kaolinite, Smec = smectite

cated from the simple water displacement from bedloads in Sr-Ca-Mg-Na-^{87}Sr/^{86}Sr space illustrated in figure 9. The calculated fraction of Ca remaining (γ) from the Koto time-series samples of the Marsyandi averages 0.11 ± 0.03 (1σ) which is less than half the average value estimated in Sr-Ca-Na (0.23) or Sr-Ca-Mg-^{87}Sr/^{86}Sr space (0.28, range 0.21 to 0.37). There are several possible explanations for this discrepancy all but one of which involve extra inputs of silicate Mg or outputs of K. These include 1) the weathered biotites have even lower K contents than the oxy- or hydro-biotites analyzed (table 2), 2) dissolution of an additional Mg-bearing phase not included in the primary minerals, 3) smectite contains unusually high K, 4) potassium is lost to another mineral or vegetation sink or 5) the chemical weathering fluxes and detrital particulate fluxes are not in equilibrium. In the modal calculations the amount of biotite weathering, and thus Mg, supplied to the water is essentially determined by the K content of the waters and the deficiency is made up by weathering additional primary Mg-bearing carbonate and precipitating Mg-poor secondary calcite. Significant weathering of K-bearing, Mg-poor phases K-feldspar, muscovite or illite would make the discrepancy larger.

It is only possible to match the modal mineral calculations to the secondary calcite precipitate estimates in Sr-Ca-Mg-^{87}Sr/^{86}Sr space if the Mg/K ratio of the inputs is higher than the analyzed biotites, that is the biotites contained 0.16 K compared with the analyzed value of 0.67 K per 11-oxygen formula unit. The low K contents of the analyzed biotites indicate that they may have been through a previous phase of weathering. If the biotites lost K by oxidation or hydration in the present phase of weathering this would tend to increase the waters K/Mg ratio and increase the Mg deficiency. Alternatively the Mg mass balance implied by the modeling in Sr-Ca-Mg-^{87}Sr/^{86}Sr space may be satisfied if the smectite contains 0.87 K per 11 oxygen formula unit but this is six times the average of 0.13 K and three times the maximum of 0.31 K observed in natural smectites by Dreif and Nieto (2000).
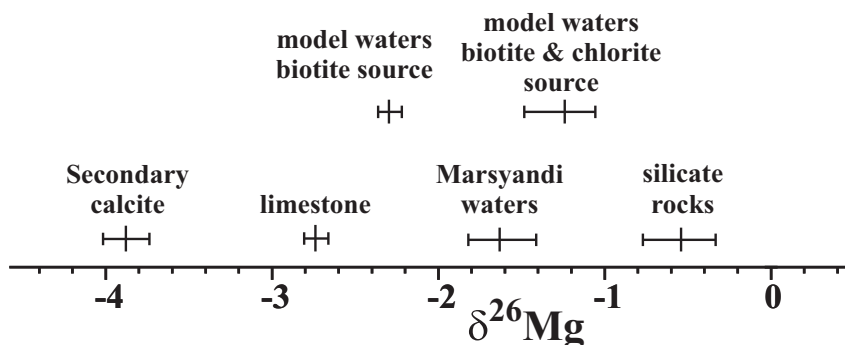
Fig. 13. Ranges of Mg-isotopic compositions measured in source rocks, secondary travertines and Marsyandi waters by Tipper and others (2006b) (lower bars) compared to range of model calculations on time-series samples for dissolution of 1) biotite alone and 2) with biotite and chlorite adjusted so that γ calculated from the mineral modes matches γ calculated from water data in Sr-Ca-Mg-^{87}Sr/^{86}Sr space. The biotite-only source requires the extra Mg to be derived from carbonate that shifts the Mg-isotopic composition to values lighter than the range of the Marsyandi waters. The composition of the smectite precipitated in these models is assumed to be $-0.5\%o$ but varying this by $\pm 1\%o$ only changes the calculated water δ^{26}Mg by $\pm 0.1\%o$.

The only significant Mg-bearing, K-poor, primary mineral is chlorite which makes up ~32 weight percent of the detrital biotite and chlorites analyzed. The average chlorite fraction of biotite plus chlorite (table 5) needs to be ~70 weight percent to increase the average calculated γ from the mineral modes to equal the value of γ calculated in Sr-Ca-Mg-^{87}Sr/^{86}Sr space.

Interestingly the time variation of the fraction of Ca remaining after precipitation of secondary calcite (γ) estimated by the mineral modal calculations (fig. 11A) is similar to that calculated in Sr-Ca-Na space (fig. 9A) and Sr-Ca-Mg-^{87}Sr/^{86}Sr space (fig. 9C) although the values are significantly smaller. Similarly the estimated ratio of chlorite to biotite as well as indicators of silicate to carbonate weathering and secondary calcite precipitation show a strong seasonal dependence consistent with the observations of Tipper and others (2006a) that the ratio of carbonate to silicate weathering increases during the monsoon. The close link between the ratio of carbonate to silicate weathering to water flux is best illustrated by the figure 11D in which the calculated ratio of Mg-carbonate to plagioclase dissolution is plotted against Na where dilution of Na is primarily a function of water flux.

A key question is whether the discrepancy between the Mg-budget calculated from the mineral modes arises from a problem with estimating inputs or outputs of Mg or K or from the estimates of secondary calcite precipitation in Sr-Ca-Na or Sr-Ca-Mg-^{87}Sr/^{86}Sr space. Below we use an additional constraint from Mg isotopes that suggests that about half the magnesium in the waters is derived from silicates.

Mg and Ca-Isotopic Compositions

The magnesium isotopic compositions of the waters and potential silicate and carbonate sources and sinks are consistent with the apparent Mg deficiency being supplied by silicate phases either in addition to that derived from biotite as constrained by the K mass balance or by loss of additional K. The Mg-isotopic compositions of rocks, bedloads and waters presented by Tipper and others (2006b) shows that Mg from the source limestone has δ^{26}Mg ~ -2.6 permil, source silicate minerals ~ -0.54 permil and the water an average δ^{26}Mg of -1.6 permil. These values imply that silicate minerals contribute ~50 percent of the Mg (fig. 13) assuming that there is no isotopic

fractionation during dissolution of Mg. Precipitation of Mg secondary calcite ($\delta^{26}Mg \sim$ $-3.8‰$) would slightly decrease this estimate, and precipitation of smectite with an enrichment factor of between $+0.5$ to 1.0 permil would slightly increase this estimate. The model with biotite as the only Mg-phase implies that only 12 percent of the water Mg is derived from silicate and predicts magnesium isotopic compositions of water in the range -2.4 to -2.2 permil, 0.7 permil lower than the Marsyandi waters. The model in which chlorite is added to biotite in a ratio to match the precipitation of secondary calcite to that calculated in Sr-Ca-Mg-^{87}Sr/^{86}Sr space predicts an average water Mg-isotopic compositions between -1.1 permil and -1.5 permil, 0.4 permil more than the analyzed values. The best match is obtained when the biotite/chlorite ratio is empirically adjusted to give $\gamma = 0.65$ of the values calculated in Sr-Ca-Mg-^{87}Sr/^{86}Sr space (0.7 of that calculated in Sr-Ca-Na space) (fig. 14). This adjustment changes the calculated ratio of Mg-bearing calcite to Mg-bearing silicates weathered where the primary control on the Mg-isotopic composition of the waters is this ratio of carbonate to silicate-derived Mg (see for example, fig. 13). By contrast the estimates of silicate to carbonate-derived Mg from the regressions in both Sr-Ca-Mg-^{87}Sr/^{86}Sr and Sr-Ca-Na space are insensitive to fixing γ at some fraction of that indicated by the regression (that is solving the regression for only the two variables F_{crb} and F_{sil}). The estimates of $\delta^{26}Mg$ in Sr-Ca-Mg-^{87}Sr/^{86}Sr space give good fits to the Mg-isotope data for a whole range of γ values whereas the estimates in Sr-Ca-Na space all deviate from the observed values (fig. 14A).

Calcium in the waters is derived almost entirely from carbonate minerals (see below); Tipper and others (2006b) inferred that the $\sim 0.15 \pm 0.10$ permil shift in $\delta^{44/42}$Ca between the limestone source and the Marsyandi waters resulted from precipitation of ~ 40 percent of the dissolved Ca as secondary calcite with a calcite-water fraction factor of ~ 0.44 permil. If the fraction of Ca lost to secondary calcite was as high as the ~ 80 percent modeled in Sr-Ca-Na space, then the observed Ca-isotopic shift would require a lower fractionation factor of ~ 0.14 permil as suggested by Tipper and others (2008). However Ca-isotopic water-calcite fractionation factors appear to result from a combination of equilibrium and kinetic factors (Lemarchand and others, 2004; DePaolo, 2011) and are not known in the Himalayas.

ALAKNANDA HIGH HIMALAYAN CRYSTALLINE SERIES AND LESSER HIMALAYAN SERIES CATCHMENTS

The catchments feeding the headwaters of the Ganges above Rishikesh, including the Dhauli Ganga, Saraswati, Alaknanda and the Bagirathi (fig. 1) were discussed in detail by Bickle and others (2005). The uppermost catchment, above Malari on the Dhauli Ganga is underlain by Tibetan Sedimentary Series and has a chemistry very similar to the Marsyandi at Chame. Regressions for this catchment against the bed-load sample AK95RS have been discussed above. The rivers then pass through the highest and most rapidly eroding section underlain by mainly amphibolite-facies silicate gneisses of the High Himalayan Crystalline Series metamorphosed during the Himalayan orogeny. The Alaknanda finally flows through a lengthy section across the lower grade phyllites, quartzites and carbonates of Lesser Himalayan Series thrust sheets.

Bed-load Samples from the Alaknanda Catchments

The bed-load samples analyzed comprise samples from catchments underlain by single tectonic units (AK95RS from the Tibetan Sedimentary Series, AK16RS and AK145M from the High Himalayan Crystalline Series Rishi Ganga catchment at Lata, AK69RS, AK74RS and AK77RS from the Lesser Himalayan Series Pinda, Nandakini and Birehi catchments) and samples from mainstem localities where river sediment and water samples comprise mixtures from more than one unit (AK43RS from
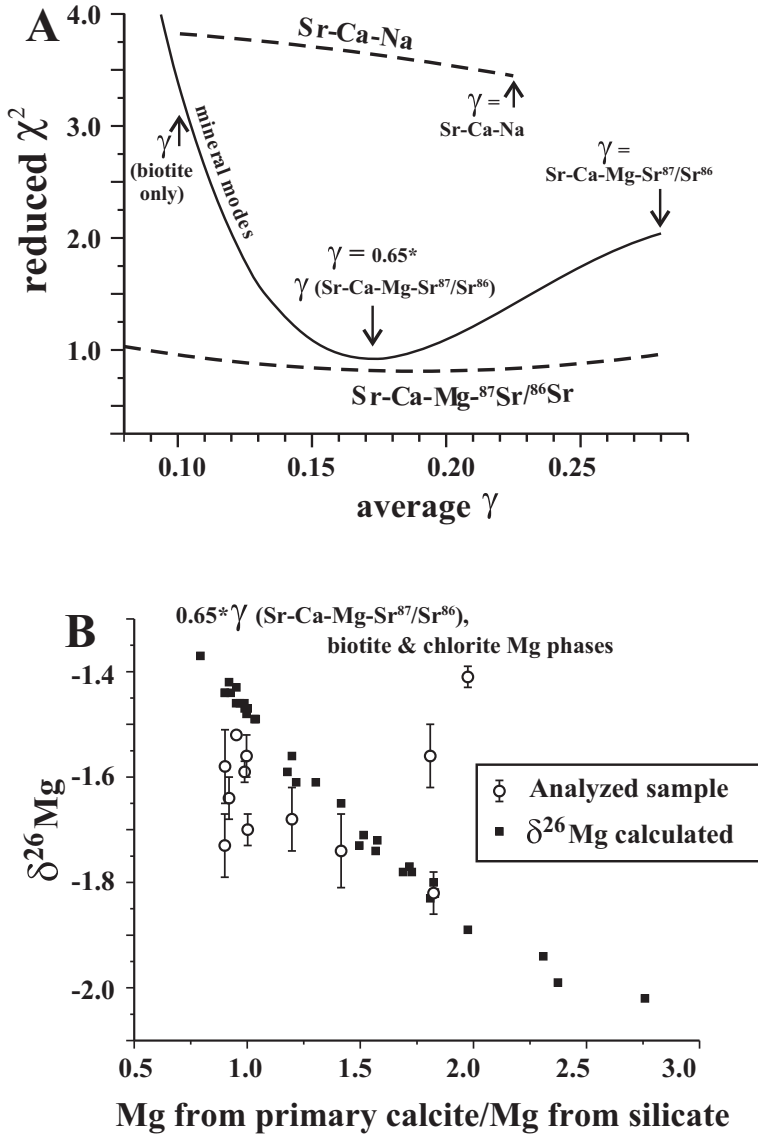
Fig. 14 (A) Solid line shows reduced χ^2 for fit of calculated $\delta^{26}Mg$ from mineral modes plotted against average fraction of Ca remaining after precipitation of secondary calcite (γ) for the set of samples analysed for $\delta^{26}Mg$ by Tipper and others (2006b). The chlorite/biotite ratio is adjusted from zero (lowest γ point) through fractions of that deduced from modeling in Sr-Ca-Mg-^{87}Sr/^{86}Sr space for each sample. The reduced χ^2 is calculated as

$$\chi_r^2 = \frac{1}{(n-1)} \sum_1^n \left(\frac{(\delta^{26}Mg - \delta^{26}Mg_C)}{\sigma} \right)^2 \tag{8}$$

where the number of samples (n = 12), $\delta^{26}Mg$ is the measured isotopic composition of the sample, $\delta^{26}Mg_C$ is the $\delta^{26}Mg$ of the sample calculated from the mineral modes for the various chlorite/biotite ratios and the mineral isotopic compositions in figure 13, σ is the estimated 1-sigma uncertainty of the $\delta^{26}Mg$ measurements (0.075‰) and γ is the mean value of γ for the full set of water samples. Dashed lines are estimates of reduced χ^2 where water $\delta^{26}Mg$ is calculated from the fractions of silicate and carbonate Mg input and Mg in secondary calcite removed calculated from regressions in Sr-Ca-Mg-^{87}Sr/^{86}Sr and Sr-Ca-Na space where γ is fixed. (B) The calculated Mg-isotopic compositions of the time-series Marsyandi waters are plotted against the ratio of Mg inputs from carbonate to Mg inputs from silicate minerals at γ calculated from mineral modes with the chlorite/biotite ratio adjusted to give $\gamma = 0.65$ times that from regression in Sr-Ca-Mg-^{87}Sr/^{86}Sr space. The analyzed $\delta^{26}Mg$ isotopic compositions of samples are plotted at the calculated ratio of carbonate-derived Mg to silicate derived Mg are also shown with 2σ error bars based on the triplicate or quadruplicate repeats of the sample analyses (Tipper and others, 2006b).

Rishikesh where the Alaknanda drains the whole mountain catchment, AK82RS from Helong on the MCT draining the High Himalayan Crystalline Series and Tibetan Sedimentary Series and AK86RS from the Saraswati which drains predominantly High Himalayan Crystalline Series with input from the Tethyan Sedimentary Series).

The bedloads from the sites that sample two or more catchments (AK82RS and AK86RS High Himalayan Crystalline Series and Tibetan Sedimentary Series and AK43RS, the whole catchment) exhibit chemistries characteristic of the mixtures. For example AK82RS sampled on the MCT has silicate residue chemistry similar to AK16RS, the small High Himalayan Crystalline Series catchment, but acetic leach chemistry (notably high Sr/Ca ratio) and Sr-isotopic composition more similar to the acetic leach of Tethyan Sedimentary Series sample AK95RS. This is explained by mixing of the high carbonate bedload from the Tethyan Sedimentary Series with the silicate-dominated bedload from the High Himalayan Crystalline Series.

As in the Marsyandi, the majority of the bedload samples and their leaches and residues lie at lower Sr/Ca ratios than the water samples (fig. 15) at a given Na/Ca ratio. The exception, AK86RS from the Saraswati, drains both Tibetan Sedimentary Series and High Himalayan Crystalline Series catchments and may well reflect imbalances between the fluxes of bedload and dissolved load from the mixed catchments. Unlike the Marsyandi bedloads and silicate residues from leaching, the compositions of the Alaknanda silicate residues from leaching lie on the correlation defined by the compositions of the whole bedload samples (fig. 4) confirming that the silicate fraction suffered no significant incongruent dissolution, during the leaching processes.

High Himalayan Rishi Ganga Catchment

The Rishi Ganga, drains a 570 km^2 catchment on the south flank of Nanda Devi entirely within High Himalayan Crystalline Series and joins the Dauli Ganga near Lata (fig. 1). Bed-load samples comprise AK16RS, a fine sand and AK145M, mud accumulated from suspended load in a pool formed as water level dropped after a rain storm during the monsoon. The suspended load sample AK145M has a similar bulk composition to the bed-load sand sample AK16RS. The acetic acid leaches of AK16RS and AK145M have Mg/Ca ratios within error of 0.105 but AK145M has a marginally higher residue Na/Ca ratio than AK16RS (2.9 compared with 2.0). The results of regressions of water compositions against either AK16RS or AK145M are well within the uncertainties arising from the estimated errors and scatter of water compositions.

Regression of the six water samples from the Rishi Ganga catchment against Sr-Ca-Mg-^{87}Sr/^{86}Sr give γ values within error of 1.0 (table 6) with the exception of sample AK92 which consistently gives γ between 1.7 and 1.8 (± 0.4 1σ) and has Na/Ca, Mg/Ca and Sr/Ca ratios double those of the other water samples. $\gamma > 1$ implies dissolution of a calcite phase with a lower Mg/Ca than input to the calculation. However the array of water compositions and bed-load leach-residue line lie very close to each other in Sr-Ca-Mg space, which makes the calculation of γ uncertain (figs. 16A and 16C). Because the bedload contains dolomite, there is uncertainty over the appropriate Mg/Ca ratio for the carbonate as the relative dissolution rates in the field will differ from laboratory acid leaches. However changing the Mg/Ca ratio of the carbonate fraction from 0.02 to 0.3 only changes the estimated average γ calculated in Sr-Ca-Mg-^{87}Sr/^{86}Sr space from 0.95 to 1.3 with a 1σ scatter of ~0.15.

As in the Marsyandi Tibetan Sedimentary Series catchment, regression in Sr-Ca-Na space gives distinctly lower estimates of γ around 0.48 implying ~50 percent of Ca is lost to secondary calcite. The time variation shows slightly higher γ values during the monsoon with both Sr-Ca-Na and Sr-Ca-Mg-^{87}Sr/^{86}Sr estimates showing similar relative amplitudes (fig. 17A). Further, there is a good correlation with the fraction of Ca lost to secondary calcite (1−γ) and water Na/Ca ratios, a proxy for the relative
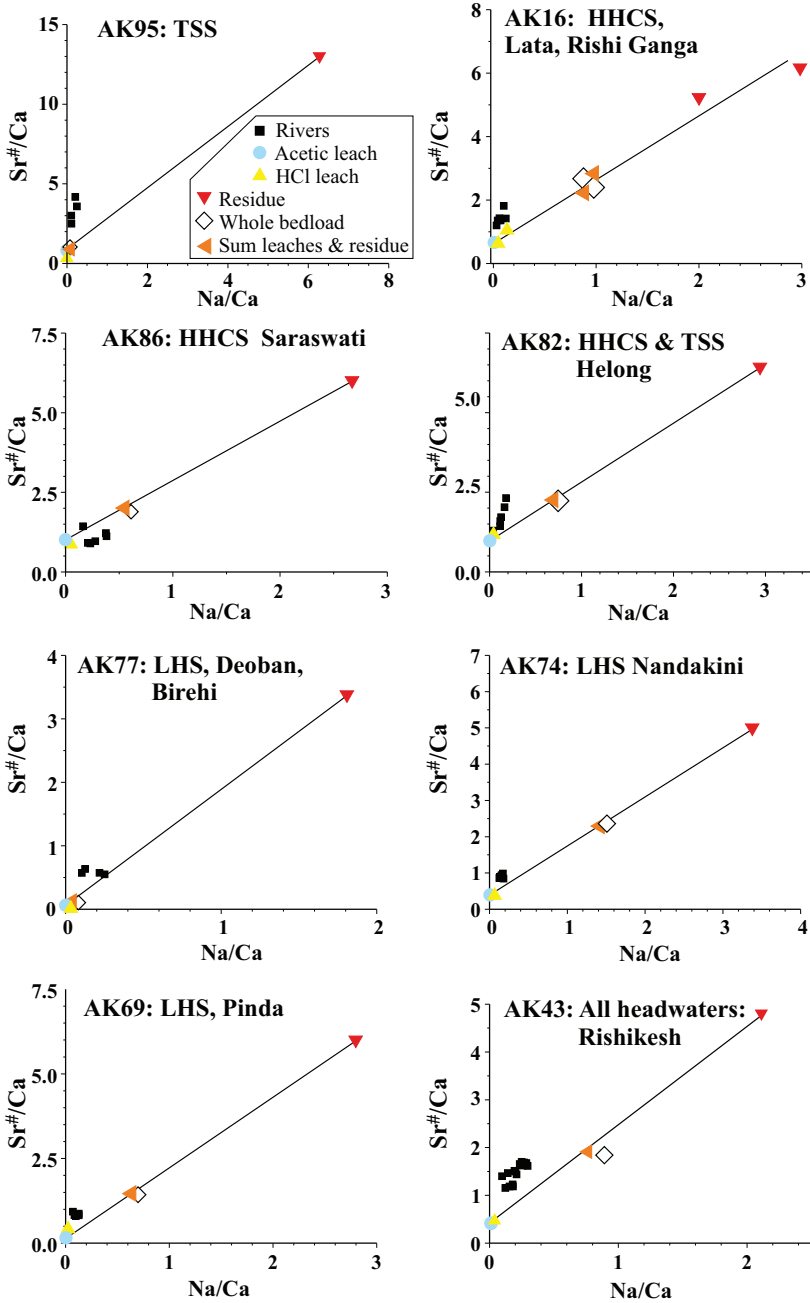
Fig. 15. Water compositions compared with bulk bed-load compositions, acetic acid leaches, residues from leaching and sum of all leach and residues (the latter compare well with the bulk bedload as a test of recovery during the leaching). Locality AK95 drains a predominantly Tethyan Sedimentary Series catchment, AK16 an High Himalayan Crystalline Series catchment and localities AK69, 74 & 77 drain Lesser Himalayan catchments. Localities AK82 (from the mainstem Alaknanda at Helong) and AK86 drain both Tethyan Sedimentary Series and HHCS catchments. AK43 is from the Alaknanda at Rishikesh where it drains the entire headwaters in the Himalayas.

Table 6

Regressions for Rishi Ganga High Himalayan Crystalline Series Catchments compared to compositions of water (mmol/L except Sr nmol/L)

Elements in regression*	χ^2 mean**	χ^2 min	χ^2 max	γ	1σ	F_{sil}	1σ	F_{crb}	1σ	Sr wat	Ca wat	Mg wat	Na wat	K wat	$^{87}Sr/^{86}Sr$ wat	%Sr sil	1σ	%Mg sil	1σ	%Ca sil	1σ
										calc	calc	calc	calc	calc	calc						
Sr-Ca-Mg-$^{87}Sr/^{86}Sr$	4.0	1.4	9.4	1.01	0.41	1.53				680	480	153	31	45	0.73709	62.3	3.1	69.0	2.8	16.6	1.8
Leach HAc***				0.16	0.07	0.51				724	480	142	199	166	0.73716						
Sr-Ca-Mg-$^{87}Sr/^{86}Sr$	10	0	25	1.2	0.33	1.15				680	480	153	31	45	0.73709	60.4	4.2	48.0	4.3	16.1	2.3
Leach HAc+HCl***				0.3	0.05	0.23				600	480	166	157	52	0.73737						
Sr-Ca-Na****				0.48	0.05	3.7				680	480	153	31	45	0.73709	8.5	1.0	11.2	1.3	1.09	0.14
HAc***				0.04	0.01	0.2						112		53	0.72539						
Sr-Ca-Mg-$^{87}Sr/^{86}Sr$	32	26	55	0.5	0.43	2.0				680	480	153	31	45	0.73709	56.7	8.3	63.7	8.0	14.0	3.7
Leach HAc$				-	0.11	0.5				799	313	154	208	176	0.73594						

* Average of samples AK16, AK114, AK145, AK200, AK259 regressed against average of AK16RS and AK145M bedload.
** Reduced χ^2 is quoted (that is χ^2 for 2 degrees of freedom divided by 2.3).
*** HAc is acetic acid leach, HAc+HCl is acetic acid leach plus silicate-corrected HCl leach.
**** Regression with three parameters gives exact solution, and exact match for the three elements fitted so only the water element concentration given for fitted elements.
$ Run with fixed $\gamma = 0.5$.
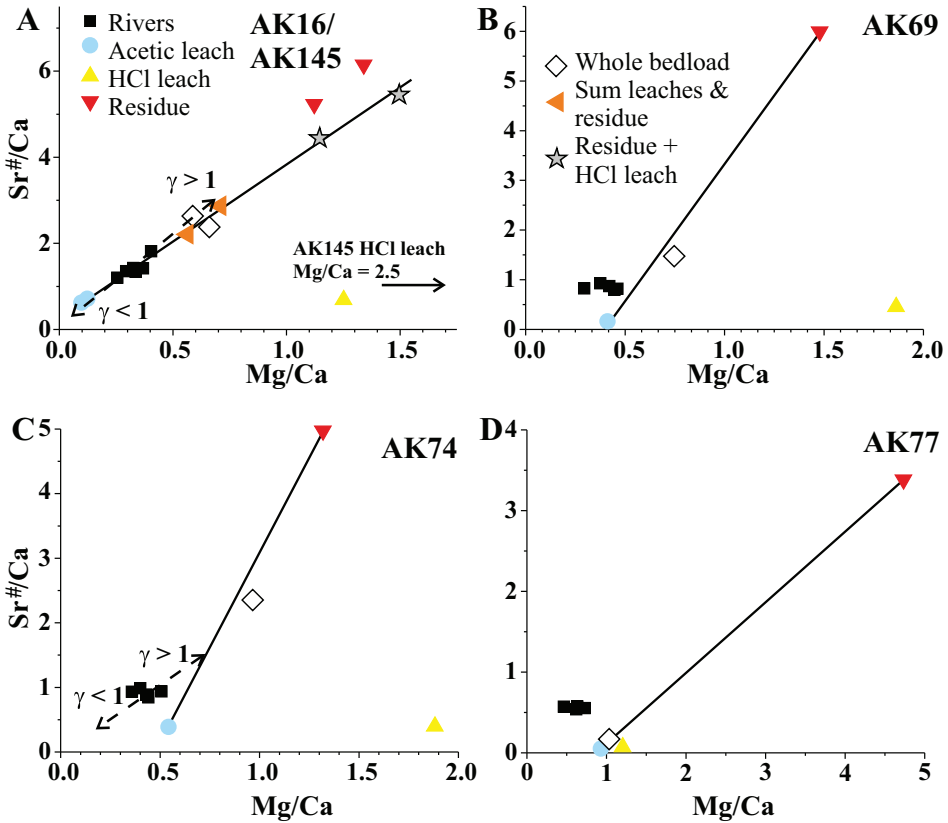
Fig. 16. (A) $Sr^{\#}/Ca$ versus Mg/Ca for High Himalayan Crystalline Rishi Ganga catchment compared to bed-load leach and residue compositions from AK16RS and AK145M. (B, C and D) $Sr^{\#}/Ca$ versus Mg/Ca for Lesser Himalayan catchments AK69RS (Pinda), AK74RS (Nandakini) and AK77RS (Birehi) compared with bed-load leach and residues. Figure 16A illustrates good match of sum of acetic and HCl leaches and residue with whole rock compositions. Dashed line in figure 16A shows trajectory as secondary calcite is precipitated ($\gamma < 1$) or added ($\gamma > 1$) and how, for these waters, the trajectory coincides with the array of water compositions and bed-load leach-residues. Figure 16C illustrates this trajectory for the Nandakini for which estimated γ is much more sensitive to carbonate Mg/Ca ratio which might be overestimated if the acetic leaches have higher Mg/Ca than the weathering ratio of calcite to dolomite in the natural waters.

magnitude of silicate chemical weathering (fig. 17B). Regression in Sr-Ca-Na-$^{87}Sr/^{86}Sr$ space exhibits a poor fit ($\chi^2 \sim 300$) compared with that in Sr-Ca-Mg-$^{87}Sr/^{86}Sr$ space (average $\chi^2 \sim 4$) suggesting that Sr-Ca-Na release is incongruent. However the apparent seasonal control on γ from both Sr-Ca-Na systematics and Sr-Ca-Mg-$^{87}Sr/^{86}Sr$ systematics is consistent with calcite precipitation exerting control on water chemistry and that the uncertain Sr-Ca-Mg-$^{87}Sr/^{86}Sr$ estimates of γ are too high. Setting $\gamma = 0.5$ and running the minimization in Sr-Ca-Mg-$^{87}Sr/^{86}Sr$ space for the two variables F_{crb} and F_{sil} gives results indistinguishable from the full regression in that space (table 6). As in the Marsyandi, the regressions in Sr-Ca-Na space give significantly smaller fractions of the cations derived from silicate minerals than the regressions in Sr-Ca-Mg-$^{87}Sr/^{86}Sr$ space (Ca $\sim 1\%$ versus 17%, Sr $\sim 9\%$ versus 60% and Mg $\sim 11\%$ versus 70%). The self-consistency of the regressions in Sr-Ca-Mg-$^{87}Sr/^{86}Sr$ space and their insensitivity to γ suggest that these provide the best estimates of fractions of silicate derived Ca, Sr and Mg.
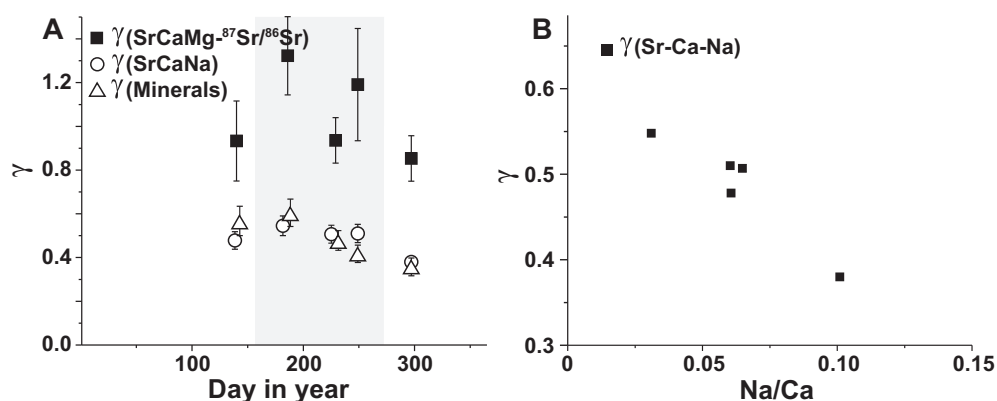
Fig. 17. (A) Variation in γ (fraction of Ca not lost to secondary calcite) calculated from regression of Sr-Ca-Mg-^{87}Sr/^{86}Sr and Sr-Ca-Na and from modal mineral decomposition for the Rishi Ganga catchment against season. Note both regressions against bedload show similar relative variations with time but differ by a factor of two in amplitude with regression in Sr-Ca-Mg-^{87}Sr/^{86}Sr space implying minimal precipitation of secondary calcite. Calculations based on modal minerals imply similar fractions of secondary calcite precipitation as calculations in Sr-Ca-Na. Monsoon denoted by gray band. (B) Variation in γ against water Na/Ca ratios from the Rishi Ganga catchment, a proxy for the fraction of cations derived from silicate weathering.

Modeling of the Rishi Ganga High Himalayan Crystalline Series Catchment Mineral Modes

Bed-load minerals from AK16RS have been analyzed by electron microprobe (table 7). The four plagioclase grains found ranged from An$_3$ to An$_{37}$, scattering around the measured Na/Ca ratios of the bed-load residues (equivalent to An$_{25}$ and An$_{33}$). The analyzed calcites have an average Mg/Ca ratio of 0.018 ± 0.01, much lower than the acetic acid leach (0.105) or the combined acetic acid and silicate-corrected HCl leaches (0.22 and 0.28). Dolomite in the bedload was not found in the grain

TABLE 7

Average composition of AK 16 bedload minerals

	Biotite	1σ	Plagioclase	1σ	Calcite	1σ	Muscovite	1σ
No*	18		4		13		3	
Si	2.74	0.03	2.76	0.16			3.12	0.03
Ti	0.13	0.03					0.032	0.080
Al	1.63	0.08	1.24	0.16			2.65	0.02
Fe	1.14	0.23	0.002	0.001	0.011	0.007	0.114	0.055
Mn	0.006	0.004			0.003	0.002		
Mg	1.23	0.25			0.017	0.009	0.085	0.025
Ca	0.05	0.04	0.245	0.159	0.969	0.017	0.001	0.001
Na	0.020	0.009	0.754	0.159			0.087	0.069
K	0.78	0.15	0.006	0.003			0.91	0.08

* Number of analyses, for analytical methods see supplementary data table S4.
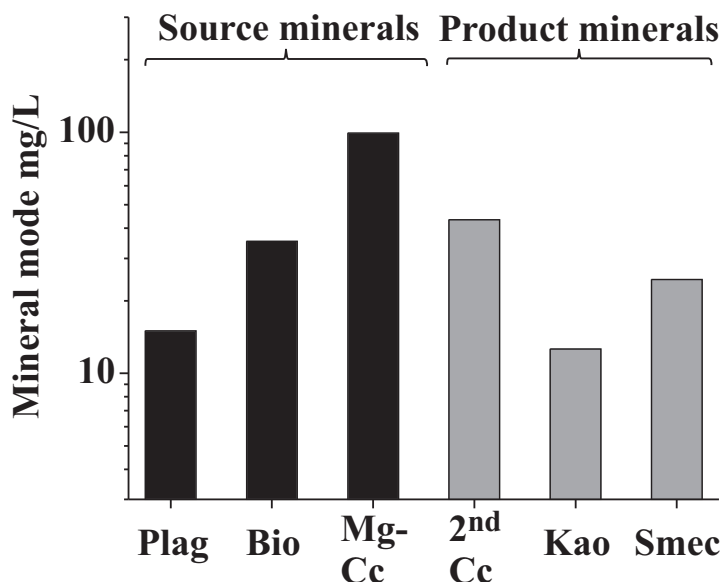
Fig. 18. Average mineral modes in mg/L calculated against bedload AK16 (AK145M gives indistinguishable results) using Mg/Ca for primary carbonate from acetic leach. Note that ~50% of carbonate is re-precipitated as secondary calcite. If Mg/Ca from acetic plus HCl leaches is used for the primary carbonate, mineral mode mass balance requires dissolution of extra Ca implying the inferred Mg/Ca ratio is higher than the ratio of the carbonate weathered. Plag = plagioclase, Bio = biotite, Chl = chlorite, Mg-Cc = primary Mg-bearing carbonate, 2nd-Cc = secondary calcite, Kao = kaolinite, Smec = smectite.

mount. However the Mg/Ca ratios of the calcites are very low and lie within the range predicted for secondary calcites precipitated from the waters of the Rishi Ganga (0.012 to 0.019 for a calcite/water Mg/Ca partition coefficient of 0.05 and precipitation of 50% of the water Ca in the secondary calcite).

Mineral mode calculations have been carried out using the acetic acid leach Mg/Ca for the Mg-carbonate component and residue Na/Ca ratios of AK16RS or AK145M for the plagioclase compositions (fig. 18). The results are insensitive to choice of plagioclase composition within this range (An_{25} to An_{33}). Using these values, the water samples from the Rishi Ganga catchment give γ values from the mineral modes and from calculations in Sr-Ca-Na space that agree within error (fig. 17). These γ values rise during the monsoon in a similar manner to the results from the Marsyandi at Koto (fig. 9A) and the Alaknanda Tethyan Sedimentary Series catchment (fig. 15F). If the Mg/Ca ratio of the combined acetic and silicate-corrected HCl leaches is used for the Mg-carbonate phase, the estimated γ is equal or greater than one, implying that this overestimates the Mg content of the inputs from weathering of the carbonate phases.

The results from the Rishi Ganga catchment thus show agreement between regressions in Sr-Na-Ca and the mineral mode calculations. These both imply that ~50 percent of Ca is lost to secondary calcite, although the $^{87}Sr/^{86}Sr$ ratio is inconsistent with this calculation, suggesting either that dissolution in Sr-Ca-Na is incongruent or ^{87}Sr is preferentially dissolved from the damaged parent Rb lattice sites. The preferential release of radiogenic isotopes from the damaged parent lattice sites could also explain the elevated fraction of Ca derived from silicate minerals based on ^{40}Ca data (Davenport and others, 2014). Regressions in Sr-Ca-Mg-$^{87}Sr/^{86}Sr$ space provide poor constraints on the magnitude of secondary calcite precipitation but are internally

consistent and fit the water data adequately when run at $\gamma = 0.5$, as inferred both from the array in Sr-Na-Ca space and from the mineral mode calculations.

Lesser Himalayan Catchments

The Lesser Himalayan catchments (AK69 Pinda, AK74 Nandakini and AK77 Birehi) contain abundant dolomite and Mg/Ca ratios in the acetic leach range from 0.42 to 0.95 and from 0.53 to 1.0 in the combined acetic and silicate-corrected HCl leach.

Regressions of Sr-Ca-Na-^{87}Sr/^{86}Sr give relatively good fits (average χ^2 between $\sim$2.5 and 16) with γ values of $\sim$0.21 (AK69RS Nandakini), 0.54 (AK74RS Pinda) and 0.39 (AK77RS, Birehi) (table 8). Calculated γ values in Sr-Ca-Mg-^{87}Sr/^{86}Sr space with carbonate compositions of the acetic leach are about one with relatively poor fits ($\chi^2 \sim$177 and 84 in the Nandakini and Pinda catchments). In the Birehi catchment the regressions yield high γ values ($\sim$10) that implies net dissolution of a carbonate with Mg/Ca less than the leach composition (see fig. 16). To match γ values in Sr-Ca-Na-^{87}Sr/^{86}Sr space, Mg/Ca ratios of the acetic leach need to be reduced from 0.42 to 0.08 (AK69RS), 0.54 to 0.18 (AK74RS) and 0.95 to 0.08 (AK77RS) that substantially improves the quality of the fits (χ^2 between 4 and 9). The percentage of silicate Sr is 20 percent in the Nandakini, 30 percent in the Pinda and a surprisingly high value at $\sim$70 percent in the Birehi, a calc-silicate dominated catchment. These values are insensitive to choice of Mg/Ca for the carbonate leach.

Mineral mode calculations were run with the average mineral compositions from the Marsyandi bedloads (table 5) in the absence of analyzed minerals from the Lesser Himalayan catchment bedloads. The results of the mineral mode calculations, assuming that the Mg/Ca ratio of the Mg-carbonate is equal the Mg/Ca ratio of the acetic acid leaches, all require additional dissolution of a low-Mg calcite, that is γ values >1. This again is consistent with the acetic leaches of samples with significant dolomite having higher Mg/Ca ratios than the natural waters in which calcite dissolution is proportionally faster. Figure 19 illustrates the calculated mineral modes with the Mg/Ca of the carbonate adjusted so that γ matches γ calculated in Sr-Na-^{87}Sr/^{86}Sr space.

DISCUSSION: IMPLICATIONS FOR SR SOURCES AND WEATHERING MECHANISMS

The results of both the regressions against bed-load leach and residues and the estimates of the modes of dissolved minerals reveal discrepancies between different sets of elements and Sr-isotopes within catchments and significant differences between catchments. In part this must represent incongruent dissolution and in part systematic differences between the weathering in catchments with different types of bedrock and different climates. The implications are that a simple single method for calculating the fractions of Sr, Ca and Mg derived from silicate is not available and that uncertainties remain in apportioning these elements between silicate and carbonate sources. This uncertainty maps into a comparable uncertainty in our estimates of the CO_2 consumed by silicate chemical weathering. Mg isotopic compositions offer a potential additional test, and where available in the Marsyandi Tibetan Sedimentary Series catchment, support the inference that significant Mg is derived from a low-K silicate phase.

The catchments are divided into three main types of chemical weathering characteristics in both Sr-Ca-Mg-Na-^{87}Sr/^{86}Sr space and in mineral mode calculations and these three divisions correlate with geology.

1) Water compositions from the Tibetan Sedimentary Series catchments give good fits in Sr-Ca-Mg-^{87}Sr/^{86}Sr space. In this system the catchments in the Marsyandi area (Marsyandi at Koto, upper Marsyandi catchments and the Nar) imply that between 65 and 80 percent of Ca dissolved is re-precipitated as secondary calcite and that on average $\sim$23 percent of the Sr, $\sim$1.2 percent of the Ca and 60 percent of the Mg

TABLE 8

Regressions for Alaknanda Lesser Himalayan catchments compared to compositions of waters (µmol/L except Sr nmol/L)

Elements in regression	χ^2 mean	χ^2 min	χ^2 max	γ	1σ	F_{sil}	1σ	F_{crb}	1σ	Sr wat calc	Ca wat calc	Mg wat calc	Na wat calc	K wat calc	^{87}Sr/^{86}Sr wat calc	%Sr sil	1σ	%Mg sil	1σ	%Ca sil	1σ
Sr-Ca-Na-^{87}Sr/^{86}Sr	2.3	0.0	5.3	0.21	0.10	0.02	0.01	5.0	0.4	367	431	172	44	36	0.74421	19.7	0.7	2.2	0.1	0.64	0.03
AK69RS Pinda*										373	430	827	41	78	0.74426						
Sr-Ca-Mg-^{87}Sr/^{86}Sr	177	149	210	0.98	0.02	1.0	0.02	1.1	0.7	367	431	172	44	36	0.74421	19.8	6.9	2.2	0.9	0.65	0.28
AK69RS Pinda*										89	431	195	9.4	17	0.74435						
Sr-Ca-Na-^{87}Sr/^{86}Sr	5.0	0.6	32	0.69	0.13	0.15	0.02	3.1	0.4	348	385	167	59	42	0.76253	30.0	1.4	7.8	0.5	3.3	0.2
AK74RS Nadakini**										308	387	318	67	69	0.76224						
Sr-Ca-Mg-^{87}Sr/^{86}Sr	84	51	118	1.16	0.08	0.75	0.03	1.8	0.7	348	385	167	59	42	0.76253	31	5	8.0	1.7	3.4	0.7
AK74RS Nadakini**										191	385	194	43	43	0.76286						
Sr-Ca-Na-^{87}Sr/^{86}Sr	22	0.6	52	0.39	0.86	0.13	0.12	0.55	0.12	280	499	322	83	51	0.77650	64.0	3.5	67.5	3.3	3.7	0.6
AK77RS Birehi***										238	501	317	89	88	0.77617						
Sr-Ca-Mg-Na-^{87}Sr/^{86}Sr	43	6.3	93	0.40	0.83	0.14	0.12	0.51	0.13	280	499	322	83	51	0.77650	64.5	4.7	68.0	4.4	3.8	0.9
AK77RS Birehi****										229	502	305	86	85	0.77659						

* Average of samples AK5, AK69, AK132, AK156, AK304 regressed against acetic leach and residue of AK69RS bedload.
** Average of samples AK7, AK74, AK117, AK128, AK190, AK293 regressed against acetic leach and residue of AK74RS bedload.
*** Average of Birehi samples AK10, AK77, AK141, AK149, AK273 regressed against acetic leach and residue of AK77RS bedload.
**** Regression of Birehi samples run with 8% of Mg in acetic acid leach shows consistency in Sr-Ca-Na-Mg-^{87}Sr/^{86}Sr space. Regression run in Sr-Ca-Mg-^{87}Sr/^{86}Sr space with composition of acetic leach and residue gives very poor fits ($\chi > 1200$) and unreasonable solutions with $\gamma \sim 10$ indicating that carbonate dissolved has an Mg/Ca ratio much less than the acetic acid leach.
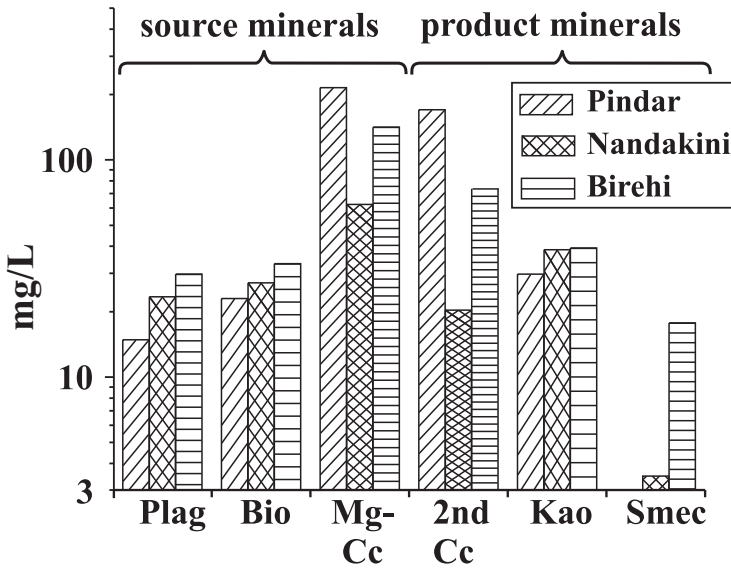
Fig. 19. Average mineral modes calculated for Lesser Himalayan catchment water samples against Marsyandi mineral compositions with plagioclase Na/Ca adjusted to match bed-load residue Na/Ca but Mg/Ca of bed-load acetic leach (carbonate) reduced to give match to the fraction of Ca remaining after precipitation of secondary calcite (γ) calculated in Sr-Ca-Na-^{87}Sr/^{86}Sr space. Note that smectite precipitation in the Pindar catchment of 0.2 gm/L plots below axis.

are derived from silicate sources. Fits to Sr-Ca-Na imply slightly more precipitation of secondary calcite (between 1 and 7% more) and that much less Ca, Sr and Mg are derived from silicate sources (on average 0.2% Ca, 4.6% Sr and 21% Mg). However fits in Sr-Ca-Na-^{87}Sr/^{86}Sr space lie substantially outside the estimated uncertainties implying that dissolution is incongruent. The Alaknanda Tibetan Sedimentary Series catchment also gives good fits in Sr-Ca-Mg-^{87}Sr/^{86}Sr space although the addition of Na to this system only degrades the fit χ^2 by a factor of four. The estimated fraction of Ca lost to precipitation of secondary calcite at 75 percent is within the range of the Marsyandi catchments but the estimated fractions of Ca, Sr and Mg derived from silicates (0.5%, 7% and 12%) are significantly less. Calculation of mineral modes consumed from deconvolution of water compositions in the Marsyandi catchment also implies precipitation of secondary calcite in amounts that significantly exceed the estimates from regression against bed-load leaches and residues. The implication, that there is a Mg-bearing, low-K phase in addition to biotite (for example chlorite), is consistent with the inference from Mg-isotope compositions and modeling in Sr-Ca-Mg-^{87}Sr/^{86}Sr space that ~50 percent of the Mg is derived from a silicate source. This conclusion is significant for silicate chemical weathering fluxes because the estimated silicate-derived Mg flux in this catchment is two orders-of-magnitude greater than the silicate-derived Ca flux.

2) The High Himalayan Rishi Ganga catchment gives regressions against bed-load leach-residues in Sr-Ca-Na space, which imply a similar fraction of secondary calcite precipitation to that estimated from mineral modes. Regressions in Sr-Ca-Mg-^{87}Sr/^{86}Sr space imply average loss to secondary calcite close to zero (that is γ ~1) but this value is poorly constrained. Interestingly the seasonal variations in γ calculated in Sr-Ca-Mg-^{87}Sr/^{86}Sr space mirror those calculated in Sr-Ca-Na space suggesting that the discrepancies result from a systematic process. Regressions in Sr-Ca-Na-^{87}Sr/^{86}Sr space are poor (average
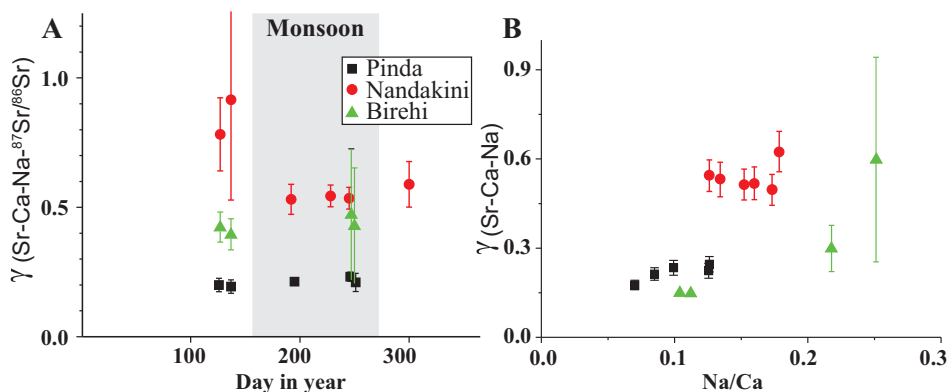
Fig. 20. (A) Variation in the fraction of Ca remaining after precipitation of secondary calcite (γ) for Lesser Himalayan catchments showing no seasonal dependence. (B) Variation in γ against water Na/Ca showing no significant correlations.

$\chi^2 \sim 1600$) suggesting incongruent dissolution in Sr-Ca-Na space or preferential dissolution of [87]Sr from damaged parent Rb lattice sites. The proportions of Ca, Sr, and Mg and derived from silicate minerals inferred from regressions in Sr-Ca-Mg-[87]Sr/[86]Sr space are about 15 percent, 60 percent and 67 percent. The magnitudes of these fractions are insensitive to reducing γ to ~0.5, compatible with displacements in Sr-Ca-Na space and mineral mode calculations. The calculated fractions of Ca, Sr, Mg derived from silicate in Sr-Ca-Na space are much smaller at 1 percent, 9 percent, and 11 percent which seems unlikely in a silicate rock-dominated catchment.

3) The Lesser Himalayan catchments have significant dolomite in the bedload and both regressions in Sr-Ca-Mg-[87]Sr/[86]Sr space and mineral mode calculations using the input carbonate with the Mg/Ca ratio of the acetic leach require additional inputs of a low-Mg calcite. However regressions in Sr-Ca-Na-[87]Sr/[86]Sr space give good fits with between 33 and 80 percent implied loss of Ca to secondary calcite. Fits in Sr-Ca-Mg-[87]Sr/[86]Sr space are consistent with this if the Mg/Ca ratios of the bedload leaches are reduced to between 10 and 33 percent of the ratio of the acetic leach implying less dissolution of dolomite. In this case, between 20 percent and 30 percent of the Sr, between 2 percent and 8 percent of the Mg and 0.3 to 3 percent of the Ca are derived from silicate sources in the Pinda and Nandakini catchments and ~4 percent of the Ca, 70 percent of the Sr and 20 percent of the Mg are silicate derived in the Birehi catchment. The Lesser Himalayan Series catchments resolve no significant seasonal variations in γ and no correlation between γ and water Na/Ca ratios (fig. 20).

Common to all the catchments is that regressions in Sr-Ca-Na and Sr-Ca-Na-[87]Sr/[86]Sr often imply more precipitation of secondary calcite and significantly lower fractions of silicate Sr and Mg than regressions in Sr-Ca-Mg-[87]Sr/[86]Sr space.

An important observation related to chemical weathering mechanisms is that the amount of secondary calcite precipitation correlates positively with the fraction of silicate weathering (figs. 7 and 17B) except in the Alaknanda Lesser Himalayan catchments. The fraction of cations supplied by silicate weathering increases during the dry season (compare Tipper and others, 2006a). This could either reflect 1) systematically more evaporation and secondary carbonate deposition during the dry season (as observed in the genetic plain, Sarin and others, 1989) which correlates with increased silicate weathering, perhaps because run off is slower or 2) mixing of two water components, one a more carbonate-dominated rapid runoff and the second a

more silicate-dominated groundwater in which a larger fraction of Ca is lost to secondary calcite precipitation. It should be noted that both the ratio of silicate input to carbonate input and the fraction of Ca lost to secondary calcite increase during the dry season. The preservation of the planar mixing arrays transposed in Sr-Ca-Na space by precipitation of secondary calcite requires that the degree of silicate weathering is positively correlated with the fraction of Ca lost to secondary calcite. If waters become rapidly saturated in calcite, the subsequent slower increase in silicate alkalinity will cause calcite precipitation as modeled for penetration of CO_2-rich waters in aquifers (Knauss and others, 2005). Such a mechanism might explain the relatively small increase in silicate cation inputs between water samples with the lowest and highest Na/Ca ratios. It is also plausible that, instead of there being two water end-members, there may be a continuum with a range of residence times (for example McGuire and others, 2005; Calmels and others, 2011), in which case the necessity for a causal relationship between silicate input and deposition of secondary carbonate to explain the planar dispositions in Sr-Ca-Na-Mg space is reinforced.

However, the reaction of carbonate-saturated waters with silicate minerals can not explain how the most carbonate-dominated waters lost ~70 percent of their Ca with implied Ca concentrations of up to ~5000 μM/l. This may have been achieved by a combination of evaporation and/or freezing in a system where CO_2 partial pressures were enhanced by microbial respiration. Alternatively cyclic changes in water chemistry along flow paths may cause repeated episodes of calcite dissolution and precipitation, concentrating the more incompatible elements, Sr and Mg in the waters as suggested by Calmels (ms, 2006).

CONCLUSIONS

The good fit of the Marsyandi time-series mainstem water samples to planes in Sr-Ca-Mg-Na- $^{87}Sr/^{86}Sr$ space is consistent with the water chemistry being dominated by mixing of inputs from carbonate and silicate end-members. Comparison of the mainstem time-series samples with the array of bed-load and rock samples in Sr-Ca-Na and Sr-Ca-Mg space implies that the water Sr/Ca ratios have been systematically increased relative to their source bedrock. We conclude that precipitation of significant amounts of secondary carbonate is the cause.

In the Tibetan Sedimentary Series catchments of the Marsyandi and Alaknanda modeling in Sr-Ca-Mg-$^{87}Sr/^{86}Sr$ space, mineral modes and of Mg-isotopic compositions predicts consistent fractions of secondary calcite precipitation and that ~60 percent of the Mg is derived from silicates. The modeling predicts that only ~1 percent of the Ca is derived from silicate and 22 percent of the Sr is silicate-derived. It also implies that dissolution of Na and K is incongruent relative to Sr-Ca-Mg with both alkalis retained. This is plausible for K held in muscovite or illite but more difficult to explain for Na, unless a significant fraction of this element is partitioned in exchangeable sites on clay minerals (Tipper and others, 2012), or perhaps precipitated as diagenetic albite.

Given the uncertainties in modeling in Sr-Ca-Na in the Tibetan Sedimentary Series catchments, it is more difficult to be confident about results from the Alaknanda High Himalayan Crystalline Series and Lesser Himalayan Series catchments as the presence of dolomite makes estimates of the Mg/Ca ratio of the carbonate component by leaching uncertain and analyses of Mg-isotopic compositions are lacking. Discrepancies in Sr-Ca-Na-$^{87}Sr/^{86}Sr$ space in the High Himalayan Crystalline Series Rishi Ganga catchment again point to incongruent dissolution although there are insufficient constraints here to determine whether this is due to Na, Mg or $^{87}Sr/^{86}Sr$. The coherence in the phase, if not in the magnitude of the amount of secondary calcite precipitation again suggests that secondary calcite precipitation is significant. All the systems modeled reflect this, (for example in Sr-Ca-Na, Sr-Ca-Na-$^{87}Sr/^{86}Sr$ and Sr-Ca-

Mg-^{87}Sr/^{86}Sr spaces and of mineral modes) implying that the factors responsible for differences in absolute fractions are systematic. The dolomite-rich Lesser Himalayan Series catchments exhibit larger discrepancies in Mg dissolution plausibly related to higher Mg/Ca ratios of acetic acid leaches than in the natural weathering solutions.

The implications are that a rigorous estimate of the fractions of silicate cations dissolved is not yet possible. The fraction of silicate Sr in the Marsyandi catchment is best constrained to be about 23 percent, around 60 percent in the High Himalayan Crystalline Series Rishi Ganga catchment and mostly between 20 and 30 percent in the Lesser Himalayan Series catchments (the Birehi catchments gives a surprisingly high fraction of at least 60%). The fraction of Mg derived from silicate minerals is around 60 percent in the Marsyandi but ~10 percent in the Alaknanda Tethyan Sedimentary Series catchment. In the Rishi Ganga High Himalayan catchment the fraction of silicate Mg is ~60 percent calculated in Sr-Ca-Mg- ^{87}Sr/^{86}Sr space but only ~12 percent calculated in Sr-Ca-Na space. Analysis of Mg and Ca isotopic compositions coupled with more reliable constraints on their isotopic fractionation factors would seem to be one way to improve these estimates.

The conclusions are that considerable uncertainties remain in the use of both element ratios and mineral modes to calculate the fractions of the major cations derived from silicate weathering with a corresponding uncertainty in the important global flux of CO_2 fixed by silicate weathering. A further complication is that secondary carbonate precipitation may also be significant to the global geochemical cycling of Ca and CO_2. Between 65 and 80 percent of the Ca is re-precipitated as carbonate within the Marsyandi and Alaknanda Tibetan Sedimentary Series catchments and about 50 percent in the Alaknanda High Himalayan Crystalline Series and Lesser Himalayan catchments. Such precipitation of secondary calcite completes the CO_2-weathering cycle on land and is not necessarily monitored by the riverine dissolved geochemical flux to the oceans. At present the ratio of secondary carbonate transported to the oceans as solids, to that re-dissolved, is not known but this ratio may be high, as secondary calcite dissolves more slowly than biogenic carbonates.

REFERENCES

Albarède, F., 1995, Introduction to Geochemical Modeling: Cambridge, Cambridge University Press, 543 p.

Andermann, C., Longuevergne, L., Bonnet, S., Crave, A., Davy, P., and Gloaguen, R., 2012, Impact of transient groundwater storage on the discharge of Himalayan rivers: Nature Geoscience, v. 5, p. 127–132, http://dx.doi.org/10.1038/ngeo1356

Berner, R. A., Lasaga, A. C., and Garrels, R. M., 1983, The carbonate-silicate geochemical cycle and its effect on atmospheric carbon dioxide over the past 100 million years: American Journal of Science, v. 283, n. 7, p. 641–683, http://dx.doi.org/10.2475/ajs.283.7.641

Bevington, P. R., and Robinson, D. K., 1992, Data reduction and error analysis for the Physical Sciences: Boston, McGraw Hill, 328 p.

Bickle, M. J., 1994, The role of metamorphic decarbonation reactions in returning strontium to the silicate sediment mass: Nature, v. 367, p. 699–704, http://dx.doi.org/10.1038/367699a0

——— 1996, Metamorphic decarbonation, silicate weathering and the long-term carbon cycle: Terra Nova, v. 8, n. 3, p. 270–276, http://dx.doi.org/10.1111/j.1365-3121.1996.tb00756.x

Bickle, M. J., Harris, N. B. W., Bunbury, J. M., Chapman, H. J., Fairchild, I. J., and Ahmad, T., 2001, Controls

on the $^{87}Sr/^{86}Sr$ of carbonates in the Garwal Himalaya, headwaters of the Ganges: The Journal of Geology, v. 109, n. 6, p. 737–753, http://dx.doi.org/10.1086/323192

Bickle, M. J., Bunbury, J., Chapman, H. J., Harris, N. B. W., Fairchild, I. J., and Ahmad, T., 2003, Fluxes of Sr into the Headwaters of the Ganges: Geochimica et Cosmochimica Acta, v. 67, n. 14, p. 2567–2584, http://dx.doi.org/10.1016/S0016-7037(03)00029-2

Bickle, M. J., Chapman, H. J., Bunbury, J., Harris, N. B. W., Fairchild, I. J., Ahmad, T., and Pomiès, C., 2005, Relative contributions of silicate and carbonate rocks to riverine Sr fluxes in the headwaters of the Ganges: Geochimica et Cosmochimica Acta, v. 69, n. 9, p. 2221–2240, http://dx.doi.org/10.1016/j.gca.2004.11.019

Blum, J. D., Gazis, C. A., Jacobson, A. D., and Chamberlain, C. P., 1998, Carbonate versus silicate weathering in the Raikhot Watershed within the High Himalayan Crystalline Series: Geology, v. 26, n. 5, p. 411–414, http://dx.doi.org/10.1130/0091-7613(1998)026<0411:CVSWIT>2.3.CO;2

Burbank, D. W., Blythe, A. E., Putkonen, J., Pratt-Sitaula, B., Gabet, E., Oskin, M., Barros, A., and Ojha, T. P., 2003, Decoupling of erosion and precipitation in the Himalayas: Nature, v. 426, p. 652–655, http://dx.doi.org/10.1038/nature02187

Caldeira, K., Arthur, M. A., Berner, R. A., and Lasaga, A. C., 1993, Cooling in the Cenozoic: Discussion of 'Tectonic forcing of late Cenozoic climate' by Raymo, M. E., and Ruddiman, W. F.: Nature, v. 361, p. 123–124, http://dx.doi.org/10.1038/361123b0

Calmels, D., MS, 2006, Altération chimique des carbonates: Influence des sources d'acidité sur les bilans globaux: Paris, France, Unpublished Diplôme de Docteur del l'Univeristé Paris 7, 248 pages.

Calmels, D., Galy, A., Hovius, N., Bickle, M., West, A. J., Chen, M. C., and Chapman, H., 2011, Contribution of deep groundwater to the weathering budget in a rapidly eroding mountain belt, Taiwan: Earth and Planetary Science Letters, v. 303, n. 1–2, p. 48–58, http://dx.doi.org/10.1016/j.epsl.2010.12.032

Chamberlin, T. C., 1899, The influence of great epochs of limestone formation upon the constitution of the atmosphere: The Journal of Geology, v. 6, n. 6, p. 609–621, http://dx.doi.org/10.1086/608185

Colchen, M., Le Fort, P., and Pecher, A., 1986, Notice explicative de la Carte Geologique Annapurna-Manaslu-Ganesh (Himalaya du Nepal) au 1:200.000ème: Paris, Éditions du Centre National de la recherche Scientifique, 138 p.

Davenport, J., Caro, G., and France-Lanord, C., 2014. Tracing silicate weathering in the Himalaya using the ^{40}K-^{40}Ca system: A reconnaissance study: Procedia Earth and Planetary Science, v. 10, p. 238–242, http://dx.doi.org/10.1016/j.proeps.2014.08.030

DePaolo, D. J., 2011, Surface kinetic model for isotopic and trace element fractionation during precipitation of calcite from aqueous solutions: Geochimica et Cosmochimica Acta, v. 75, n. 4, p. 1039–1056, http://dx.doi.org/10.1016/j.gca.2010.11.020

Drever, J. I., 1994, The effect of land plants on weathering rates of silicate minerals. Geochimica et Cosmochimica Acta, v. 58, n. 10, p. 2325–2332, http://dx.doi.org/10.1016/0016-7037(94)90013-2

—— 1997, The geochemistry of natural waters: Upper Saddle River, Prentice Hall, 436 p.

Drief, A., and Nieto, F., 2000, Chemical composition of smectites formed in clastic sediments. Implications for the smectite–illite transformation: Clay Minerals, v. 35, n. 4, p. 665–678, http://dx.doi.org/10.1180/000985500547124

Edmond, J. M., 1992, Himalayan tectonics, weathering processes, and the strontium isotope record in marine limestones: Science, v. 258, n. 5088, p. 1594–1597, http://dx.doi.org/10.1126/science.258.5088.1594

English, N. B., Quade, J., DeCelles, P. G., and Garzione, C. N., 2000, Geologic control of Sr and major element chemistry in Himalayan rivers, Nepal: Geochimica et Cosmochimica Acta, v. 64, p. 2549–2566, http://dx.doi.org/10.1016/S0016-7037(00)00379-3

Gabet, E. J., Burbank, D. W., Pratt-Sitaula, B., Putkonen, J., and Bookhagen, B., 2008, Modern erosion rates in the High Himalayas of Nepal: Earth and Planetary Science Letters, v. 267, n. 3–4, p. 482–494, http://dx.doi.org/10.1016/j.epsl.2007.11.059

Gabitov, R. I., and Watson, E. B., 2006, Partitioning of strontium between calcite and fluid: Geochemistry, Geophysics, Geosystems, v. 7, n. 11, p. Q11004, http://dx.doi.org/10.1029/2005GC001216

Gaillardet, J., Dupré, B., Louvat, P., and Allegre, C. J., 1999, Global silicate weathering and CO_2 consumption rates deduced from the chemistry of large rivers: Chemical Geology, v. 159, n. 1–4, p. 3–30, http://dx.doi.org/10.1016/S0009-2541(99)00031-5

Galy, A., and France-Lanord, C., 1999, Weathering processes in the Ganges-Brahmaputra basin and the river alkalinity budget: Chemical Geology, v. 159, n. 1–4, p. 31–60, http://dx.doi.org/10.1016/S0009-2541(99)00033-9

Galy, A., France-Lanord, C., and Derry, L. A., 1999, The strontium isotopic budget of Himalayan Rivers in Nepal and Bangladesh: Geochimica et Cosmochimica Acta, v. 63, n. 13–14, p. 1905–1925, http://dx.doi.org/10.1016/S0016-7037(99)00081-2

Garrels, R. M., and Mackenzie, F. T., 1967, Origin of the chemical composition of some springs and lakes, *in* Gould, R. F., editor, Equilibrium Concepts in natural Water Systems: Advances in Geochemistry, v. 67, chapter, 10, p. 222–242, http://dx.doi.org/10.1021/ba-1967-0067.ch010

Harris, N. B. W., Bickle, M. J., Chapman, H. J., Fairchild, I., and Bunbury, J., 1998, The significance of Himalayan rivers for silicate weathering rates: evidence from the Bhoti Kosi tributary: Chemical Geology, v. 144, n. 3–4, p. 205–220. http://dx.doi.org/10.1016/S0009-2541(97)00132-0

Jacobson, A. D., Blum, J. D., and Walter, L. M., 2002, Reconciling the elemental and Sr isotope composition of Himalayan weathering fluxes: Insights from the carbonate geochemistry of stream waters: Geochimica et Cosmochimica Acta, v. 66, n. 19, p. 3417–3429, http://dx.doi.org/10.1016/S0016-7037(02)00951-1

Knauss, K. G., Johnson, J. W., and Steefel, C. I., 2005, Evaluation of the impact of CO_2, co-contaminant gas, aqueous fluid and reservoir rock interactions on the geologic sequestration of CO_2: Chemical Geology, v. 217, n. 3–4, p. 339–350, http://dx.doi.org/10.1016/j.chemgeo.2004.12.017

Krishnaswami, S., and Singh, S. K., 1998, Silicate and carbonate weathering in the drainage basins of the Ganga-Ghaghara-Indus head waters: contributions to major ion and Sr isotope geochemistry: Proceedings of the Indian Academy of Sciences - Earth and Planetary Sciences, v. 107, p. 283–291.

Krishnaswami, S., Trivedi, J. R., Sarin, M. M., Ramesh, R., and Sharma, K. K., 1992, Strontium isotopes and rubidium in the Ganga-Brahmaputra river system: Weathering in the Himalaya, fluxes to the Bay of Bengal and contributions to the evolution of oceanic $^{87}Sr/^{86}Sr$: Earth and Planetary Science Letters, v. 109, p. 243–253, http://dx.doi.org/10.1016/0012-821X(92)90087-C

Krishnaswami, S., Singh, S. K., and Dalai, T. K., 1999, Silicate weathering in the Himalayas: role in contributing to major ions and radiogenic Sr to the Bay of Bengal, *in* Somayajulu, B. L. K., editor, Ocean Science, trends and future directions: New Dehli, Indian National Science Academy and Akademi Book International, p. 23–51.

Lemarchand, D., Wasserburg, G. J., and Papanastassiou, D. A., 2004, Rate-controlled calcium isotope fractionation in synthetic calcite: Geochimica et Cosmochimica Acta, v. 68, n. 22, p. 4665–4678, http://dx.doi.org/10.1016/j.gca.2004.05.029

Lupker, M., France-Lanord, C., Galy, V., Lavé, J., Gaillardet, J., Prasad Gajurel, A., Guilmette, C., Rahman, M., Kumar Singh, S., and Sinha, R., 2012, Predominant floodplain over mountain weathering of Himalayan sediments (Ganga basin): Geochimica et Cosmochimica Acta, v. 84, p. 410–432, http://dx.doi.org/10.1016/j.gca.2012.02.001

Maher, K., Steefel, C. I., White, A. F., and Stonestrom, D. A., 2009, The role of reaction affinity and secondary minerals in regulating chemical weathering rates at the Santa Cruz Soil Chronosequence, California: Geochimica et Cosmochimica Acta, v. 73, n. 10, p. 2804–2831, http://dx.doi.org/10.1016/j.gca.2009.01.030

McGillen, M. R., and Fairchild, I. J., 2005, An experimental study of incongruent dissolution of $CaCO_3$ under analogue glacial conditions: Journal of Glaciology, v. 51, n. 174, p. 383–390, http://dx.doi.org/10.3189/172756505781829223

McGuire, K. J., McDonnell, J. J., Weiler, M., Kendall, C., McGlynn, B. L., Welker, J. M., and Seibert, J., 2005, The role of topography on catchment-scale water residence time: Water Resources Research, v. 41, n. 5, p. W05002, http://dx.doi.org/10.1029/2004WR003657

Melo, V. F., Singh, B., Schaefer, C. E. G. R., Novais, R. F., and Fontes, M. P. F., 2001, Chemical and mineralogical properties of kaolinite-rich Brazilian Soils: Soil Science Society of America Journal, v. 65, n. 4, p. 1324–1333, http://dx.doi.org/10.2136/sssaj2001.6541324x

Müller, G., 1969, High strontium contents and Sr/Ca-ratios in Lake Constance waters and carbonates and their sources in drainage area of Rhine river (Alpenrhein): Mineralium Deposita, v. 4, n. 1, p. 75–84, http://dx.doi.org/10.1007/BF00206650

Négrel, P., Allègre, C. J., Dupré, B., and Lewin, E., 1993, Erosion sources determined by inversion of major and trace element ratios and strontium isotopic ratios in river water: The Congo Basin case: Earth and Planetary Science Letters, v. 120, n. 1–2, p. 59–76, http://dx.doi.org/10.1016/0012-821X(93)90023-3

Nehrke, G., Reichart, G.-J., Van Cappellen, P., Meile, C., and Bijma, J., 2007, Dependence of calcite growth rate and Sr partitioning on solution stoichiometry: Non-Kossel crystal growth: Geochimica et Cosmochimica Acta, v. 71, n. 9, p. 2240–2249, http://dx.doi.org/10.1016/j.gca.2007.02.002

Nielsen, L. C., De Yoreo, J. J., and DePaolo, D. J., 2013, General model for calcite growth kinetics in the presence of impurity ions: Geochimica et Cosmochimica Acta, v. 115, p. 100–114, http://dx.doi.org/10.1016/j.gca.2013.04.001

Oliver, L., Harris, N., Bickle, M., Chapman, H., Dise, N., and Horstwood, M., 2003, Silicate weathering rates decoupled from the $^{87}Sr/^{86}Sr$ ratio of the dissolved load during Himalayan erosion: Chemical Geology, v. 201, n. 1–2, p. 119–139, http://dx.doi.org/10.1016/S0009-2541(03)00236-5n

Palmer, M. R., and Edmond, J. M., 1992, Controls over the strontium isotope composition of river water: Geochimica et Cosmochimica Acta, v. 56, n. 5, p. 2099–2111, http://dx.doi.org/10.1016/0016-7037(92)90332-D

Press, W. H., Flannery, B. P., Teulolsky, S. A., and Vetterling, W. T., 1986, Numerical Recipes: Cambridge, Cambridge University Press, 818 p.

Price, J. R., Heitmann, N., Hull, J., and Szymanski, D., 2008, Long-term average mineral weathering rates from watershed geochemical mass balance methods: Using mineral modal abundances to solve more equations in more unknowns: Chemical Geology, v. 254, n. 1–2, p. 36–51, http://dx.doi.org/10.1016/j.chemgeo.2008.05.012

Raymo, M. E., and Ruddiman, W. F., 1992, Tectonic forcing of late Cenozoic climate: Nature, v. 359, p. 117–122, http://dx.doi.org/10.1038/359117a0

Raymo, M. E., Ruddiman, W. F., and Froelich, P. N., 1988, Influence of late Cenozoic mountain building on ocean geochemical cycles: Geology, v. 16, n. 7, p. 649–653, http://dx.doi.org/10.1130/0091-7613(1988)016<0649:IOLCMB>2.3.CO;2

Richter, F. M., Rowley, D. B., and DePaolo, D. J., 1992, Sr isotope evolution of seawater: the role of tectonics: Earth and Planetary Science Letters, v. 109, n. 1–2, p. 11–23, http://dx.doi.org/10.1016/0012-821X(92)90070-C

Rimstidt, J. D., Balog, A., and Webb, J., 1998, Distribution of trace elements between carbonate minerals and aqueous solutions: Geochimica et Cosmochimica Acta, v. 62, n. 11, p. 1851–1863, http://dx.doi.org/10.1016/S0016-7037(98)00125-2

Sarin, M. M., Krishnaswami, S., Dilli, K., Somayajulu, B. L. K., and Moore, W. S., 1989, Major ion chemistry of the Ganga-Brahmaputra river system: Weathering processes and fluxes to the Bay of Bengal: Geochimica et Cosmochimica Acta, v. 53, n. 5, p. 997–1009, http://dx.doi.org/10.1016/0016-7037(89)90205-6

Searle, M. P., and Godin, L., 2003, The South Tibetan Detachment and the Manaslu Leucogranite: A Structural Reinterpretation and Restoration of the Annapurna-Manaslu Himalaya, Nepal: The Journal of Geology, v. 111, n. 5, p. 505–523, http://dx.doi.org/10.1086/376763

Singh, S. K., Trivedi, J. R., Pande, K., Ramesh, R., and Krishnaswami, S., 1998, Chemical and strontium, oxygen, and carbon isotopic compositions of carbonates from the Lesser Himalaya: Implications to the strontium isotope composition of the source waters of the Ganga, Ghaghara, and the Indus rivers: Geochimica et Cosmochimica Acta, v. 62, n. 5, p. 743–755, http://dx.doi.org/10.1016/S0016-7037(97)00381-5

Tesoriero, A. J., and Pankow, J. F., 1996, Solid solution partitioning of Sr^{2+}, Ba^{2+}, and Cd^{2+} to calcite: Geochimica et Cosmochimica Acta, v. 60, n. 6, p. 1053–1063, http://dx.doi.org/10.1016/0016-7037(95)00449-1

Thien, B. M. J., Kulik, D. A., and Curti, E., 2014, A unified approach to model uptake kinetics of trace elements in complex aqueous – solid solution systems: Applied Geochemistry, v. 41, p. 135–150, http://dx.doi.org/10.1016/j.apgeochem.2013.12.002

Tipper, E. T., ms, 2006, The isotopic fingerprint of calcium and magnesium: from the alteration of the continental crust to global budgets: Cambridge, United Kingdom, University of Cambridge, Unpublished Ph. D. thesis, 233 pages.

Tipper, E. T., Bickle, M. J., Galy, A., West, A. J., Pomiès, C., and Chapman, H. J., 2006a, The short term climatic sensitivity of carbonate and silicate weathering fluxes: Insight from seasonal variations in river chemistry: Geochimica et Cosmochimica Acta, v. 70, n. 11, p. 2737–2754, http://dx.doi.org/10.1016/j.gca.2006.03.005

Tipper, E. T., Galy, A., and Bickle, M. J., 2006b, Riverine evidence for a fractionated reservoir of Ca and Mg on the continents: Implications for the oceanic Ca cycle: Earth and Planetary Science Letters, v. 247, n. 3–4, p. 267–279, http://dx.doi.org/10.1016/j.epsl.2006.04.033

Tipper, E. T., Galy, A., and Bickle, M. J., 2008, Calcium and Magnesium isotope systematics in rivers draining the Himalaya-Tibetan-Plateau region: Lithological versus fractionation control?: Geochimica et Cosmochimica Acta, v. 72, n. 4, p. 1057–1075, http://dx.doi.org/10.1016/j.gca.2007.11.029

Tipper, E. T., Calmels, D., Gaillardet, J., Louvat, P., Capmas, F., and Dubacq, B., 2012, Positive correlation between Li and Mg isotope ratios in the rivers of the Mackenzie Basin challenges the interpretation of apparent isotopic fractionation during weathering: Earth and Planetary Science Letters, v. 333–334, p. 35–45, http://dx.doi.org/10.1016/j.epsl.2012.04.023

Turchyn, A. V., Tipper, E. T., Galy, A., Lo, J., and Bickle, M. J., 2013, Isotope evidence for secondary sulfide precipitation along the Marsyandi River, Nepal, Himalaya: Earth and Planetary Science Letters, v. 374, p. 36–46, http://dx.doi.org/10.1016/j.epsl.2013.04.033

Vance, D., Bickle, M. J., Ivy-Ochs, S., and Kubik, P. W., 2003, Erosion and Exhumation in the Himalaya from cosmogenic isotope inventories of river sediments: Earth and Planetary Science Letters, v. 206, n. 3–4, p. 273–288, http://dx.doi.org/10.1016/S0012-821X(02)01102-0

Walker, J. C. G., Hays, P. B., and Kasting, J. F., 1981, A negative feedback mechanism for the long-term stabilization of Earth's surface temperature: Journal of Geophysical Research-Oceans, v. 86, n. C10, p. 9776–9782, http://dx.doi.org/10.1029/JC086iC10p09776

West, A. J., Bickle, M. J., Collins, R., and Brasington, J., 2002, Small catchment perspective on Himalayan weathering fluxes: Geology, v. 30, n. 4, p. 355–358, http://dx.doi.org/10.1130/0091-7613(2002)030<0355:SCPOHW>2.0.CO;2

West, A. J., Galy, A., and Bickle, M. J., 2005, Tectonic and Climatic Controls on Silicate Weathering: Earth and Planetary Science Letters, v. 235, n. 1–2, p. 211–228, http://dx.doi.org/10.1016/j.epsl.2005.03.020

White, A. F., and Brantley, S. L., 2003, The effect of time on the weathering of silicate minerals: why do weathering rates differ in the laboratory and field?: Chemical Geology, v. 202, n. 3–4, p. 479–506, http://dx.doi.org/10.1016/j.chemgeo.2003.03.001

White, A. F., Schulz, M. S., Vivit, D. V., Blum, A. E., Stonestrom, D. A., and Anderson, S. P., 2008, Chemical weathering of a marine terrace chronosequence, Santa Cruz, California I: Interpreting rates and controls based on soil concentration–depth profiles: Geochimica et Cosmochimica Acta, v. 72, n. 1, p. 36–68, http://dx.doi.org/10.1016/j.gca.2007.08.029

Wolff-Boenisch, D., Gabet, E. J., Burbank, D. W., Langner, H., and Putkonen, J., 2009, Spatial variations in chemical weathering and CO_2 consumption in Nepalese High Himalayan catchments during the monsoon season: Geochimica et Cosmochimica Acta, v. 73, n. 11, p. 3148–3170, http://dx.doi.org/10.1016/j.gca.2009.03.012

Zachos, J., Pagani, M., Sloan, L., Thomas, E., and Billups, K., 2001, Trends, rhythms, and aberrations in global climate 65 Ma to present: Science, v. 292, n. 5517, p. 686–693, http://dx.doi.org/10.1126/science.1059412